Patient-specific Virtual Ultrasound Imagery for

Virtual Reality Simulation of Central Line Placement

BY
XIAORUI ZHAO

B.S., Huazhong University of Science & Technology, 2007
M.S., Zhejiang University, 2010

THESIS

Submitted as partial fulfillment of the requirements
for the degree of Doctor of Philosophy in
Industrial Engineering and Operations Research
in the Graduate College of the
University of Illinois at Chicago, 2015

Chicago, Illinois

Defense Committee:

Prashant P. Banerjee, Chair and Advisor
Cristian J. Luciano
David He
Alexandra Van Meter, Internal Medicine
Ron C. Gaba, Radiology

TABLE OF CONTENTS

CHAPTER **PAGE**

LIST OF TABLES

TABLE **PAGE**

LIST OF FIGURES

FIGURE **PAGE**

LIST OF FIGURES (continued)

FIGURE **PAGE**

LIST OF ABBREVIATIONS

API	Application Program Interface
CLABSI	Central-Line Associated Bloodstream Infections
CT	Computed Tomography
CUDA	Compute Unified Device Architecture
CVC	Central-line Venous Catheterization
DICOM	Digital Imaging and Communications in Medicine
DOF	Degree of Freedom
FEM	Finite Element Method
FOV	Field of View
GLSL	OpenGL Shading Language
GPU	Graphics Processor Unit
GUI	Graphic User Interface
IJV	Internal Jugular Vein
MPR	Multiplanar Reconstruction
MRI	Magnetic Resonance Imaging
PET-CT	Positron Emission Tomography–Computed Tomography
SAIL	Stanford Artificial Intelligence Laboratory
SCP	Surface Contact Point
SIMD	Single Instruction Multiple Data

LIST OF ABBREVIATIONS (continued)

SDK	Software Development Kit
US	Ultrasound
VR	Virtual Reality
VRML	Virtual Reality Modeling Language
XML	Extensible Markup Language

SUMMARY

Ultrasonography can be a very useful tool for medical diagnosis and treatment. Ultrasound imagery is used to visualize internal anatomical structures as an intuitive visual guidance for various non-invasive procedures. The goal of this dissertation is to develop a simulator that incorporates ultrasound visualizations and mirrors or enhances a real clinical situation with guided experiences in an interactive manner. This technique, used in pre-surgical planning and residents training, will improve the residents' performance and increase their confidence while economically complement the traditional manikin or cadaver-based training process. The broader impact of the research undertaking is to formulate the ultrasound visualization as an off-the-shelf component that is plugged into any surgical environment including complex human anatomies. A proof-of-concept implementation is demonstrated by a procedure known as central line venous catheterization. This percutaneous procedure, performed by multiple specialties, consists of inserting a needle that will guide a catheter into a large vein located in the targeted site for administering medication or fluids, or obtaining blood tests or cardiovascular measurements. Mostly used in the internal jugular approach, ultrasound imagery provides visual guidance for the surgeon to recognize the internal anatomical structure of the neck, as well as the position and orientation of the needle being inserted. A characteristic collapse of the vein, produced when applying slight pressure to the skin with the ultrasound transducer, helps the surgeon differentiate vein from artery, as the latter does not collapse. During training with the simulator, residents are able to develop the kinesthetic and psychomotor skills required for this bimanual procedure inserting the needle with one hand while properly manipulating the ultrasound transducer with the other. Pre-surgical planning of challenging cases of patients with abnormal anatomy can also be conducted with this patient-specific simulator.

Introduction

The Proposed Study

Ultrasound (US) has been the main technique for clinic palpation and procedural guidance. As an imaging modality, ultrasound possesses the advantage of fast temporal resolution, low cost, and portability, and thus remains the primary practice for patient diagnosis even after the invention of CT/MRI technology. Even though on-line ultrasound imaging simulation was raised for more than a decade ago, but it has not been extensively explored and implemented. Virtual ultrasound would facilitate surgical learning on a virtual model rather than on a manikin or a cadaver, allowing us to work on a specific patient anatomy and at the same time to reduce training costs. When performing a procedure, surgeons need to be aware of anatomical features of the region. A successful surgery outcome relies heavily on real-time hand-eye coordination with high fidelity graphical and haptic feedback. The location and orientation of the transducer are important to obtain a useful ultrasound image that is able to aid the surgeon to properly place the surgical equipment in the correct location. Thus, a good understanding from the image acquisition will only have practical standing in a real-time domain, while the surgeon's interaction with the virtual patient entails the outstanding performance of the simulation with high graphical and haptic resolution to justify the procedural operation. Unfortunately, this has not been considered in the past. The purpose of the ultrasound project described in this thesis is to develop a simulator that generates the ultrasound image from CT patient dataset in real time, and provide sufficiently accurate visual guidance, while guarantee the realism of the haptic interaction using virtual reality and haptic technology. The real-time change due to the interaction between the

surgical device and the anatomical structure is also properly considered to reflect the realism of the simulation.

Intellectual Merit

This research work provides a change in the paradigmatic framework for surgical simulation by being able to easily and realistically re-create ultrasound guided surgical environment. Either for training of novices or for providing pre-surgical planning to experts, the simulator takes CT images of a real patient and displays a stereoscopic view of the 3D virtual upper torso and neck, including skin, muscle, bone, organs, veins, and arteries using CUDA language. The simulator detects the contacts between the surgical instruments (needle and transducer) and the volumetric iso-surfaces that represent multiple layers of soft and hard tissues of the patient anatomy using a volume haptics algorithm. Both instruments are controlled by two SensAble® Phantom haptic devices that provide realistic force feedback to the user in a graphics/haptics collocated augmented reality environment. A GPU-based ray-casting algorithm efficiently processes in parallel the CT volume of that particular patient and renders a dynamic virtual ultrasound image using GLSL. Visual effects of ultrasonic reflection and absorption, as well as soft tissue deformation and vein vessel collapse, are displayed by the computer-generated image providing a highly realistic ultrasound guided CVC simulator.

Broader Impacts of the Proposed Research

The proposed study leads to an immersive simulator that renders the ultrasound based palpation and surgical environment. It is able to overcome the limitations of the traditional training performed with a real ultrasound machine and a plastic mannequin or an actual patient. The real-

time effects rendering of different anatomical regions of the patient body are displayed all in real-time with abundant details adapting to different requirement of the procedures. The estimation of the deformation will be interfaced with the virtual model and human interface input from the external haptic devices. With stereoscopic graphics rendering and haptic feedback, the surgeon is able to obtain a realistic experience of the specific procedure. The further research results of the acoustic characteristics of the human body can be easily plugged into the simulator as it has been parameterized and interfaced. Also it provides a broaden horizon for different procedures simulation with ultrasound. The innovative methodology that the ultrasound image is generated in real time together with the deformation estimation and integration makes it suitable for any training environment, and will act as a more interactive tool for the surgeons in the pre-surgical planning. With a better acknowledge of the graphical and physical characteristics of the image, the research is valuable in both surgical and educational fields.

Background and Related Work

Background and Motivation

Ultrasound (US) is the historical modality that was firstly documented by Loomis and Wood in the 1920s as having a biologic effect on living tissues [1]. Therapeutic ultrasound technology integrated with the imaging is now one of the most rapidly expanding techniques that has replaced many traditional surgical procedures as minimally invasive image-guided approach [2]. various image modalities used to provide intuitive guidance, such as Computed Tomography (CT) and Magnetic Resonance Imaging (MRI), the US often facilitates procedures that require real-time rendering of the anatomy and is, thus, often registered with other modalities for intra-operative purposes [3-5]. The ultrasound is also well known for advantage of affording high-resolution guiding without radiation and at relatively low costs [6-8], after the development for more than at least a decade, it has become an economical, safest and widely available approach to carry out common procedures including biopsies, drainages, and percutaneous injections. The US-guided percutaneous injections can be provided by probes or using a freehand technique, to inject substances into infectious lesions, tumors and pathologically abnormal region inside human body [9, 10].

While “ultrasound guidance for interventional procedure is versatile and has applications throughout the body” [11], the real-time simulation of ultrasound is “based on acquisition of actual ultrasound images and creating a compounded 3D volume of the region of interest” [12-14]. The ultrasound images were previously acquired from an actual ultrasound system. In real-time, the simulator then played back ultrasound images that were generated based on the interpolation of the pre-recorded image stack [15, 16], according to the various placements of the

probe during the navigation. A number of previous simulation platforms, including commercialized simulators, were derived for ultrasound training thereafter, and provided reasonable efficacy for the interventional procedures. These simulators provide a framework of ultrasound imaging on various anatomy modules, which registers corresponding mannequin with an extensive patient case model database, and fall into different interventional radiology disciplines. The volume based training simulators utilize an image volume to reconstruct the ultrasound image slice, are unable to provide haptic feedback from different patient or pathological surfaces. [12-14, 17-22]. These historical off-line simulators also share the common shortcoming of no processing of the image. This is especially the case when "the probe is further away from the acquisition position, as there are no view-dependent artifacts such as shadowing and the effect of a fixed gain and focus, of which the fully synthetic and realistic simulation of is computationally expensive" [23]. The image realism has become the most significant bottleneck for the practical use of training for these simulators.

More recent research has taken different imaging modalities into consideration, while the development of hardware acceleration technology facilitates the on-line image generation rather than the previous pre-computed staging volume. "The use of CT images as the basis for simulations not only avoids the drawbacks of view-dependent artifacts, but also has the advantage of allowing for patient specific simulations, ease of navigation for novice users as they can practice ultrasound navigation with the help of corresponding CT information" [24]. The CT volume was adopted to visualize simple ultrasound model, and corresponding needle insertion simulation for specific training [25, 26]. A relatively enhanced ray-tracing based registered model for ultrasound "results in realistic ultrasound simulations from CT images is suitable for ultrasound training" [23, 24, 27, 28]. However, the simplified problem does not have the

capability of recording the real time changes of the surrounding tissue layout, while on the other hand, no research so far has been undertaken to cope with the visualization of the interaction between the equipment and anatomical tissues. Thus, it has increased the risk during the advancing of the inserted needle between the volume slices and guarantees the precision. “The mesh-based Finite Element Method (FEM) techniques are excellent for accurate deformation calculations, but unsuitable for use in real-time surgical simulation” [29]. “Due to the requirement of numerical integration, they are slow and require extensive pre-computation for speedup” [29]. The majority of the existing simulators for ultrasound guided interventional procedures [30] have to find a trade-off between the volumetric rendering as well as the ray-casting algorithms, and the sufficiently achievable image resolution for the ultrasound image computation. “A conceptually viable implementation was recently presented in [23], combining both an estimation of acoustic properties from CT data similar with [31] and a scatter image texture computed using FIELD II algorithm” [32]. Nevertheless, no SIMD (Simple Instruction Multiple Data) approach was taken into account to meet the requirements of the real-time simulation and interaction. A GPU approach using NVidia’s CUDA architecture [33] has paved the path to the interaction implementation, which few of the current research has been involved yet. The overall performance is approached by sacrificing the quality on either side, and the outcome would be far from satisfactory. Thus, the realism of the region that is relatively distant from the acquisition point cannot be guaranteed or could only be circumvented.

Therefore, a simulator that provides high fidelity haptic feedback with the volumetric model of the patient, while incorporating real-time intra-operative generation of ultrasound image, is needed for the training and pre-surgical planning purposes. In order to provide enough information, the acoustic characteristics in CT scanned images are well exploited to register into

the ultrasound image for the necessity of ultrasound display. Under the special scenario of minimal or non-invasive procedures, the deformable ultrasound image is, hence, indispensable to satisfy the real-time operation during the probe penetration.

Ultrasound Guided Central Line Placement Procedure Introduction

Central line placement, also known as central venous catheterization (CVC) is a historical and tested technique to quickly access the major venous circulation system. "The procedure of inserting a central venous catheter was initially reported by Werner Forssman, a surgical intern who describes canalizing his own right atrium via cephalic vein in 1929" [34]. And the technique that became the paradigmatic was subsequently introduced by Sven-Ivar Seldinger in 1953 [34]. This proposed technique revolutionized the discipline of medicine by fast and easy access of central venous system [35]. "The indication of CVC procedure is that it allows the placement of various types of intravenous lines for fluids infusion, blood products and drugs to obtain blood for laboratory analysis" [36].

"Three common types of central veins insertion sites are most used for venous access include the subclavian, femoral and internal jugular vein (IJV), subclavian vein and. And three traditional access approaches are used for the IJV access: anterior, posterior and central, of which the latter two are most commonly used that can minimize the chance in vascular puncture. The capacity to place a central line in the IJV is an important skill; this is the preferable vein for placement of a trans-venous pacemaker as it is a straight line down the vein to the right side of the heart" [36] .

Bedside ultrasonography has reshaped the general technique of the central venous catheter placement in both internal jugular vein and femoral vein approach, while the subclavian

approach retains the commonly used blind approaches. The use of ultrasonography is often helpful for the visualization of Internal Jugular Vein (IJV) and carotid artery, regardless of the access approach to the IJV [37-40]. Real-time two-dimensional ultrasound guidance is superior to blind, landmark-guided techniques, particularly when used during CVC insertion into the internal and subclavian veins, in terms of reducing insertion failure, arterial puncture, hematoma and hemothorax. From the observed result of reducing the chance of complications, ultrasound is increasingly used as the guidance for accurate placement of the needle. While static ultrasound can be used to localize the vein for access when using techniques that rely on knowledge of anatomic landmarks, dynamic ultrasound can be used to guide the needle into the targeted vein in real-time. Familiarity with ultrasound-guided access is a critical aspect for the practitioner performing frequent central venous access procedure, such that the acquisition of the spatial reasoning and hand-eye coordination skills requires a specialized training process.

Proposed Work

The majority tasks performed in radiology are carried out based on two dimensional information, presented by various modalities from x-ray imaging to more advanced CT, PET-CT or MRI. Radiologist can have effortless and sophisticated volumetric tool at their disposal to interpret digital images, with a substantial amount of volume datasets. Volumetric rendering and analysis "allow the radiologist or consulting physician to select the best possible view of the finding in question for accurate diagnosis, interpretation and determination of the best treatment strategy concerning specific patient" [41]. Volumetric data is physically a three-dimensional matrix of scalar or vector data, it can store information about both the surface and inside of the object. With the transition process from analog to digital imaging, the emerging voxelisation [42]

process create a discretised cubic model of an object consisting of voxels that are closely fit together, with a corresponding resampled numeric value. This section introduces the methods of obtaining volume data from 3D scanning raw data from spiral CT machines.

Volumetric Data Processing and Rendering

Volume Data Preprocessing and Patient Specific Models Generation

There are two types of the volumes related to the current work: one is used as the input of the deformable ultrasound rendering pipeline; the other is used for CUDA accelerated volumetric rendering and provide a high quality volume display for haptic interaction. Both are obtained from CT scan image, while the formal type of the volume is post-processed into two volumes used for different purposes: the original volume and the binary mask. Color transfer function is used to process the voxel data explicitly stored in the volumetric dataset and derived from it to find a RGBA value. Each voxel in the volumetric dataset is assigned a color value and an opacity value. This classification can be viewed as a form of pattern recognition [43].

The original volume is obtained from a dataset of CT DICOM images. This volume is used to simulate the natural echoic image of anatomical structure. The resolution of the imagery depends on the capabilities of the CT scanner and the protocol to follow for the particular surgical procedure. CT imaging is recorded in 16-bit imaging and converted to 8-bit to reduce GPU (Graphical Processing Unit) memory and computational requirements. Therefore, grey-scale values from 0 to 255 correspond to the density of the tissue (Figure 1).

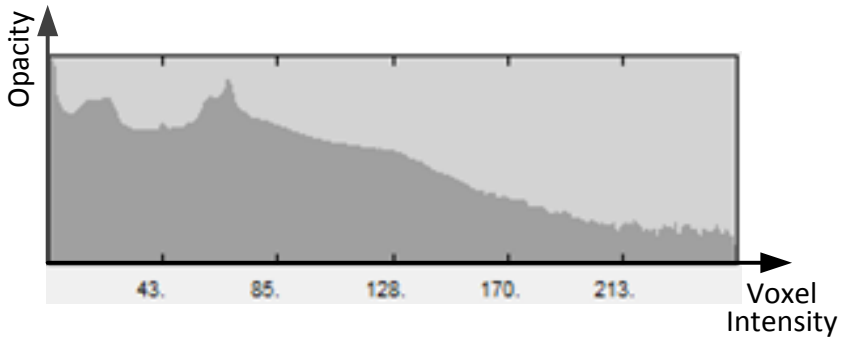

Figure 1. Histogram of the intensity opacity map.

The distribution of values is used for the realistic appearance of the ultrasound image rendering. The ultrasound is displayed using a customized transfer function that properly displays the pixel information from the graph above. Each pixel is correlated to a specific tissue density. For example, the density of skin can be found around value 45, compared to bone around value 200. In order to better visualize vein and arteries, a CT dataset with contrast is usually requested. However, the contrast dye affects the opacity of the vessels in the CT, making them look the same as bone. While image fusion technique is not cost effective way, as it always involves post processing efforts for a better registration between different modalities. Thus, in order to overcome this problem, manual segmentation is performed to separate specific anatomy: bone, vein, artery, etc.

Besides the original volume, a customized mask volume is also retrieved, in which the distinct individual anatomical structures are assigned labels during the segmentation process. This classification process is utilized to convert arbitrary scalar data into categorized visual properties. This information is needed to know what anatomy is interacting with the transducer and if it will deform when applying pressure with the virtual transducer. The mask volume histogram has a variant contour form compared to the original volume, as the voxels of the same type are aggregated to specific intensity with opacity coefficients as height in vertical axis, and appear as numerous dark gray clusters (cf. Fig. 2). Table 3.1 shows an example of the label results obtained after segmentation.

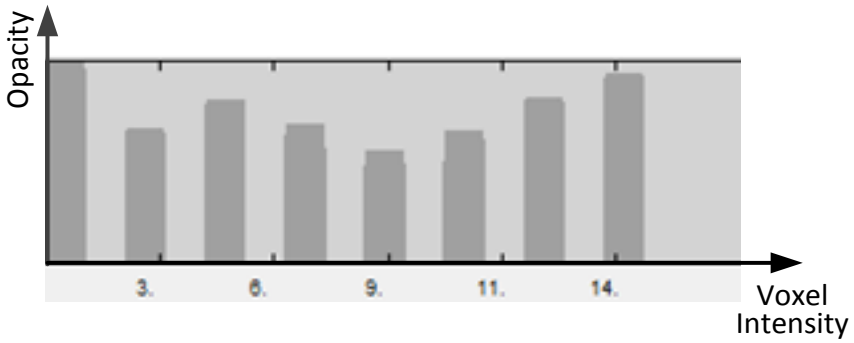

Figure 2. Mask volume intensity-opacity map.

An open source toolkit named VolView [44], specialized on visualizing and analyzing 3-D medical and scientific data, is used to fulfill the volume retrieving objective. These two volumes

are imported into the virtual scene and precisely collocated with the previously mentioned CUDA volume for the further image rendering.

3-D Patient Volume Visualization and Interaction

The concept of iso-surfaces involves the "extraction of an intermediate representation that approximates the surface of relevant objects from volume data set" [45]. This is done by choosing a value that can produce an iso-surface by rendering only the specific voxels that are falling within the selected value threshold. The outcome of isosurfacing process often pertains to a polygonal mesh, in particular a triangular mesh, which is used to represent the boundary of an object and can be efficiently rendered by graphic hardware.

The latter type of the volume mentioned in the previous section is used to generate mesh objects based on the volumetric data. The most popular algorithm is Marching Cubes [46, 47]. Numerous variations of this algorithm have been developed since its proposal. It has become the first priority of medical applications to adopt and take advantage of this technique [48]. A modified marching cubes algorithm in nVidia's CUDA language is designed to generate independent isosurfaces for different anatomical structures. This algorithm takes the voxel positions from the volume and produce triangular iosurfaces at the same location. This generated mesh is further used to render different tactile effects with the instruments. A Gaussian filtering strategy is applied to make the surface smoother and, thus, improve the user's haptic experience.

Ultrasound Imagery and Effect Simulation

Obtaining the Clipped 2-D Image for Ultrasound

Once the volume geometries are rendered with decent frame rate, the slicing of the clipped images is considered. A slightly different strategy from the ultrasonography is proposed to update the intersected tissue display on the beam plane of the ultrasound transducer. The goal is to visualize two-dimensional oblique interpolated slices from original CT scan dataset stack in parallel directions. A virtual camera object is introduced to track the transform of the field of view of the camera that is corresponding to the virtual transducer to format resulting images in real time.

When using the convex curvilinear array transducer in the actual ultrasound guided procedures, the piezoelectric material [49] at the bottom of the transducer emits sector-shaped beams which forms a plane. While in the simulation, this plane is interpolated by a set of the clipped slices from the view volume. The slice stack is precisely aligned with the sector plane: the virtual perspective camera node is mounted right above the plane and faced downward. The rotation of the camera is carefully defined so that the lateral border of the ultrasound image is consistent with the lateral border of the transducer (cf. Fig. 3). The margin between the near and far distance attributes of the camera defines the depth of the image stack clipped. The depth is set to an optimal value to guarantee the resolution of the image, as it fuses the consecutive slices and merge all the clipped isosurfaces into one single compounded image. The height angle attribute is set to scale the field of view region for the image. After the configuration, the camera is transformed corresponding to the placement of the transducer in global view and generates a 2D image of the clipped volume and carry out perspective rendering.

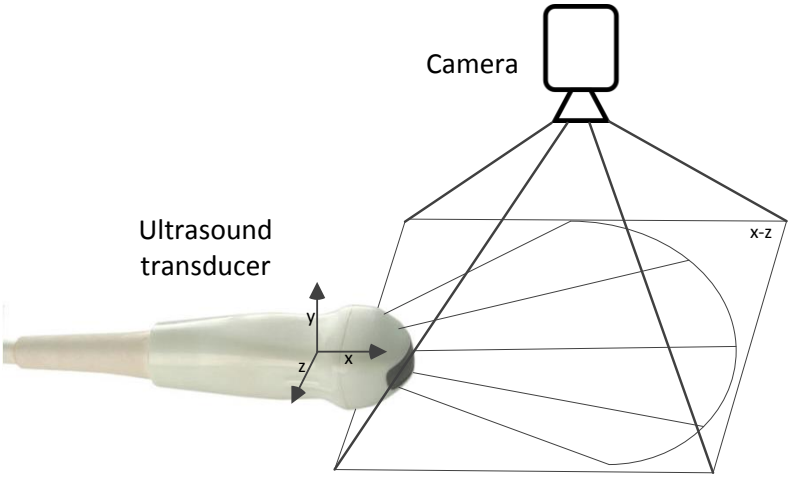

Figure 3. Camera placement with respect to the transducer.

The volumetric dataset and ultrasound imagery, as a collection of geometric objects, are inserted into a database called scene graphs, the internal states of which are traversed and queried in a sequence by the computer programs to display and update the scene in real time. "Scene graphs are data structures used to hierarchically organize and manage the contents of spatially oriented scene data, it has become popular as a general purpose mechanism for managing a variety of media types" [50]. This data structure has been adopted by many programs and APIs including OpenSceneGraph [51], OpenSG [52], VRML 97 [53] (Virtual Reality Modeling Language), X3D [54] and Open Inventor [55].

In order to reduce the complexity of the GPU computation codes, Open Inventor Graphics SDK is utilized to render the perspective that the camera captures. Open Inventor is an advanced object-oriented toolkit for OpenGL programming. The lower level atomic instructions that are sent to the GPU devices are encapsulated into node classes. The nodes including the fundamental manipulation (transformation, texture generation and binding, lighting, etc.) are organized into a

scene graph, and work in discipline to render the "virtual world". The ultrasound image rendering of the soft tissue mainly includes the development of two classes derived from Open Inventor nodes: *SoTissueDeformationShader* and *SoUltrasoundShader*. Both classes contain internal GLSL shader implementation for photorealistic ultrasound image rendering.

SoTissueDeformationShader: This node (cf. Fig. 4) stores the clipped image slices from both the original volume and the segmented volume in corresponding texture unit group node. These two types of images will be passed to a GLSL shade for the vertex and fragment rendering in parallel. The shader uses 2D coordinates to access the pixel within both images and replace the fragment color of current pixel by that of another pixel at the computed position after deformation. The output of the shader will be used to render a rectangle shape under the entire scene as the input to the second developed node as below.

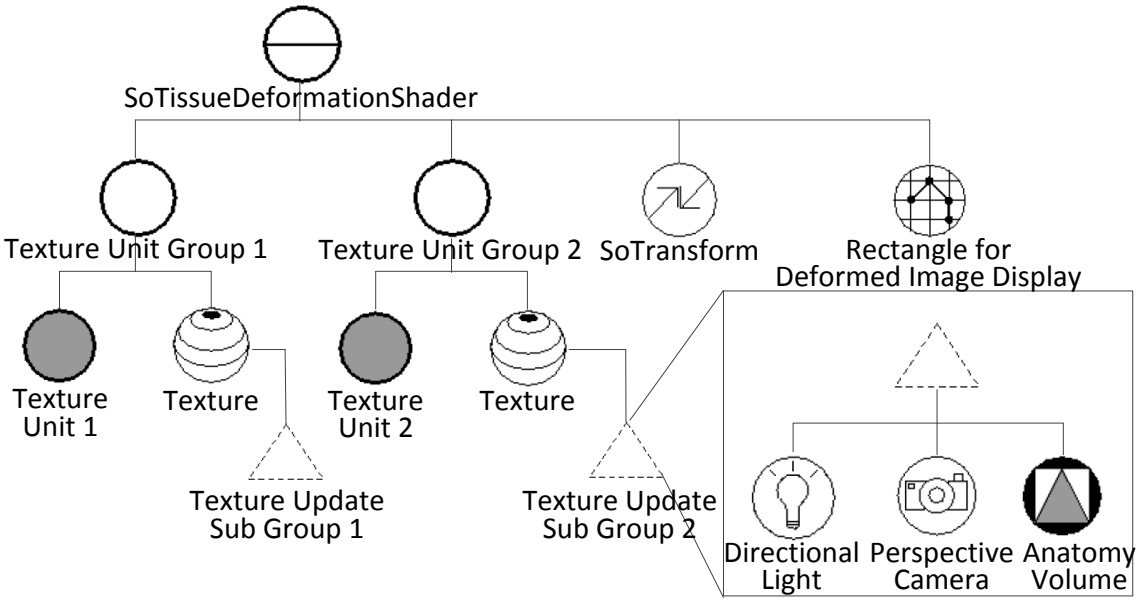

Figure 4. Scene graph of deformation computation.

SoUltrasoundShader: This node (cf. Fig. 5) specifically deals with the ultrasound effect rendering. Now that the previous deformed tissue image is already rendered onto the geometry, this geometry is located under a scene texture node, which will also be passed to the internal GLSL shader to render the ultrasound effect. The scene texture node is necessary, instead of the ordinary texture node, since there is no way to read out the content inside an active texture unit because of an Open Inventor limitation. Thus, this texture buffer cannot be transferred to the shader directly. After the ultrasound effect rendering, the texture will be eventually visualized onto the quad in the virtual scene as the final ultrasound image.

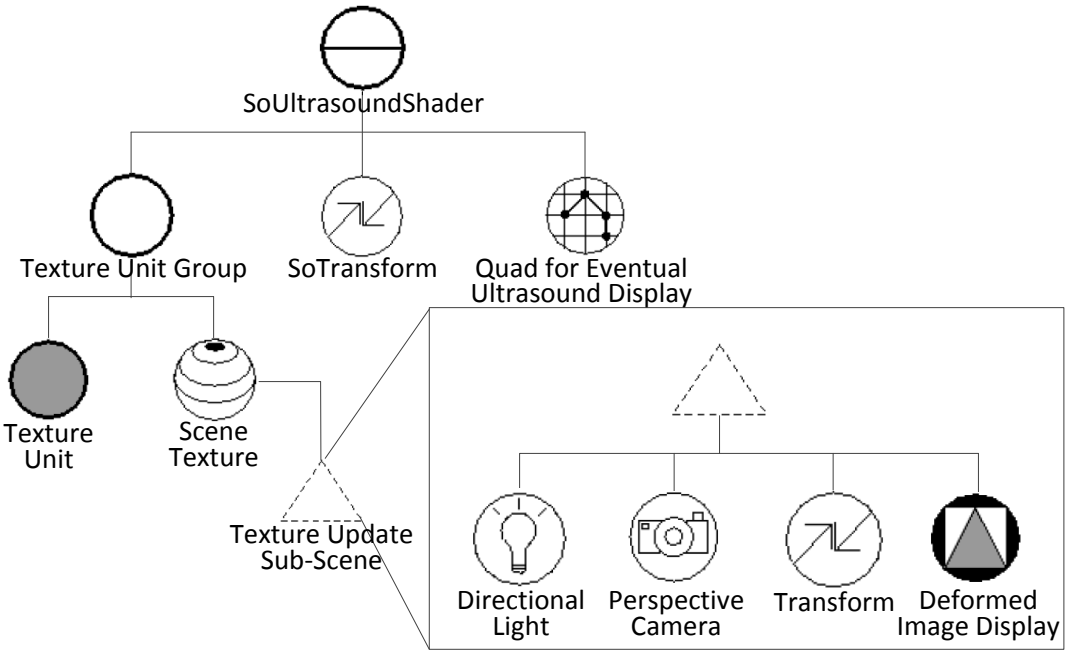

Figure 5. Scene graph of ultrasound rendering.

In summary, the original clipped images from both volumes will go through a two-phase rendering pipeline: first phase for tissue deformation rendering in particular, in the second phase the internal shader uses the rendering scene from the first phase and generates the result ultrasound image.

Tissue Deformation Modeling

As the initial step, Young's Modulus properties for different tissues are collected from the previous publications (cf. table I), which indicates the "elasticity of a material to resume its original size and shape after being subjected to a deforming force or stress" [56]. The Young's Modulus parameters are correspondent to the label indices of mask volume as in section 2.1, and passed to the GLSL shader as an index map, so that the shader is able to find out the elasticity of the pixel using its label index in parallel.

TABLE I
PARAMETERS OF SEGMENTED VOLUME

Tissue Category	Young's Modulus (kPa)	Label Number	Remark
Background	INF	0	
Artery	200 [11, 14]	2	interpolated
Lungs & trachea	1000	4	varies
Vein	23 [11, 14]	6	interpolated
Thyroid	800 [15]	8	
Sternocleidomastoid muscle (SCM)	100 [16]	10	
Bones	14000 [12]	12	
Everything else	80	14	interpolated

A mass-spring system prototype has been adopted and implemented to represent deformation of soft tissue. As illustrated in figure 6, the bottom line of the 2-D image is considered as the farthest end of the field of view region that the force transmission can reach, and thus no deformation is applied. The clipped plane of the upper body volume is firstly divided into parallel columns, widths of which are equal to the dimension of one single pixel. Each pixel along the columns inside the rectangular image is treated as an equivalent spring, and initially assigned a unit length. Under a contact force at one single point on the skin surface, the spring system will be compressed, and the deformation extent of every point inside the tissue is represented by a computed coefficient with respect to the original length of that pixel. According to the Hook's Law, each pixel has an output for the shrunk length (as L'_{ij} in Fig. 6), depending on the Young's modulus factor as its physical metric.

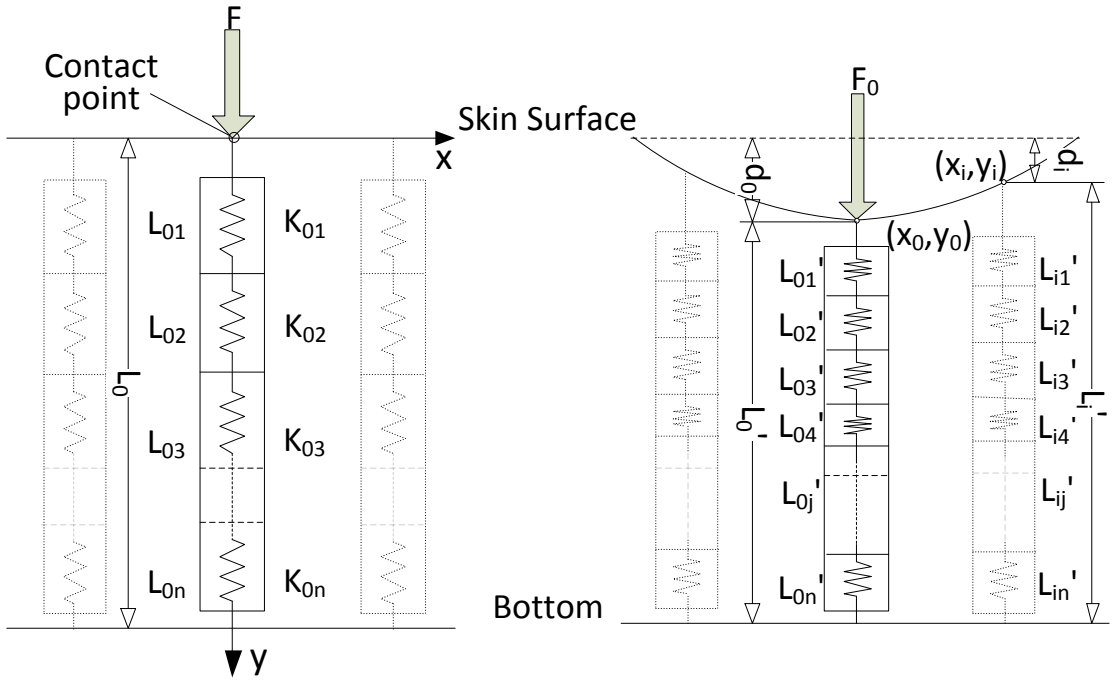

Figure 6. Mass-spring approximation of soft tissue deformation.

The surface contact force and internal distributed force are both considered. The contact force is retrieved from haptic loop with the touching force magnitude, while the surface deformation curve obeys a Normal distribution function. It is assumed that, the force along the column traverses through the isotropic tissue and thus remains as constant, practical distortion of the force field considering shearing strength in tangential direction is planned to be assessed as further research topic.

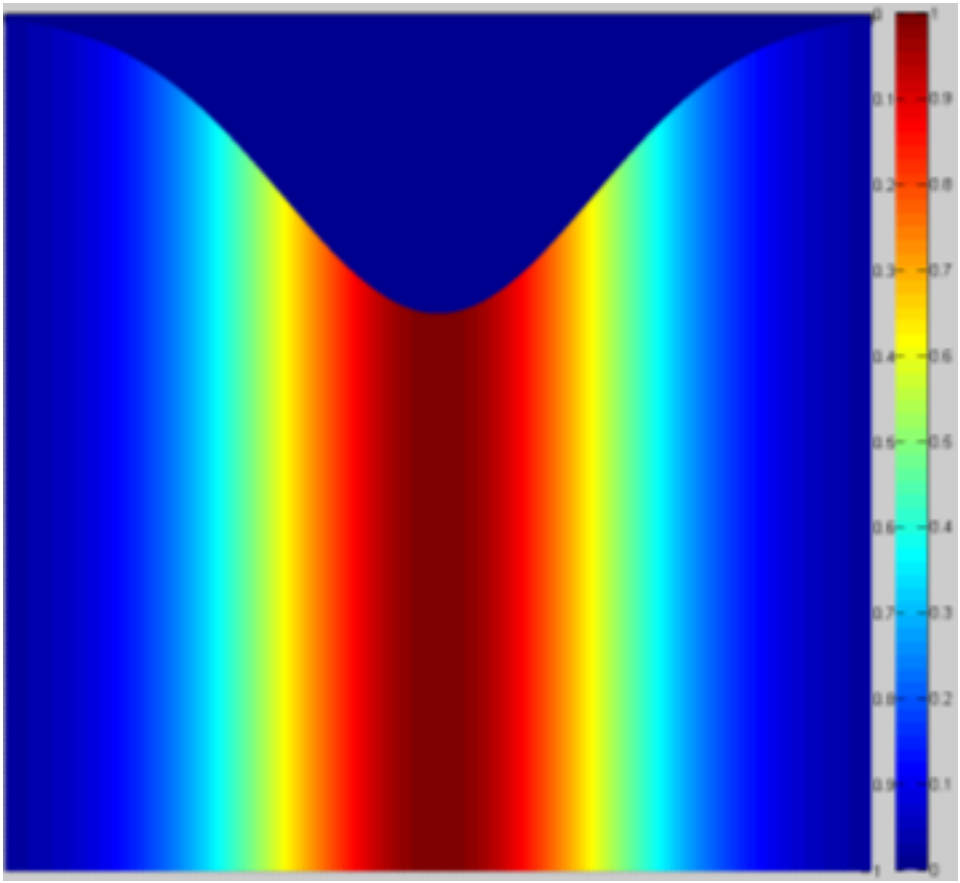

Figure 7. Force field chart with MATLAB in homogeneous tissues.

As in Figure 7, a surface contact force as well as the force distribution field in the beams plane is drawn. The distribution chart does not illustrate the interrelationship between the force and the tissue density at a specific location. Considering the actual anatomical structure on the intersection plane, it is also reasonably assumed that the skin surface will remain in a smooth contour obeying the 2-D normal distribution function. Hence, the deformation length at that particular point is used to calculate a compensated force (F_{ic} in Eqn. (3)) based on over all elasticity coefficients, the deformation of the particular pixel along the column below can be calculated accordingly.

$$d_0 = \sum_{i=1}^{n} F_0/k_{0i} \qquad (1)$$

$$d_i = d_0 * NID(\mu, \sigma^2) \qquad (2)$$

$$F_{ic} = d_i/\sum_{j=1}^{n} 1/k_{ij}, \qquad (3)$$

$$L'_{ij} = L_{ij} * - F_{ic}/k_{ij}\ , j = 1, \dots n \qquad (4)$$

$$y'_{ij} = L_0 - \sum_{k=j+1}^{n} L'_{ik} \qquad (5)$$

The above algebraic equation sets from (1)-(5) describes the computation of pixel substitution map based on the calculated surface pressure above. With original coordinate of the pixels and the deformation coefficient, the new coordinate of current pixel in vertical direction can be calculated by accumulating the lengths of all the pixels below the point (cf. eqn (5)).

Rendering of Ultrasound Effects

The acoustic characteristic within the ultrasound image can be well summarized by previous work [6, 7]. The ultrasound effect can be simulated based on 2D MPR image, which is computed from the original set of CT dataset stack. Four acoustic characteristics are compounded into the eventual rendered image: reflection, absorption, radial blur, and Perlin noise based speckle. A GPU based ray casting algorithm to render the image has been implemented in OpenGL Shading Language (GLSL).

Reflection: It is shown in the ultrasound image that clear reflections may occur at the border between different interfaces of the tissue such as bone or gas, arteries and veins, as well as fat/tissues. The differences can be observed when the acoustic resistances between two distinct adjacent tissues is larger than 0.1% [57].The reflection feature defines the ultrasound wave that echoes back to the transducer. It produces an intermediate map by detecting and enhancing edges in the deformed ultrasound image using a computing kernel. The gradient of the acoustic impedances between two adjacent pixels on incident interface is calculated. This scale is used to further compute the light intensity transmitted back to the transducer. While Snell's law [58] can be applied to the ultrasound for the intensity reflected at a specular interface, we also need to focus on the light intensity that is reflected back to the transducer, such that we consider the general diffuse besides specular reflection. The Lambert's cosine law is adopted for the ideal diffusive reflection case where the same amount of intensity is reflected in each direction along the curvature within the two dimensional ultrasound image.

$$\frac{I_r}{I_i} \approx \cos(\theta)^2 \left(\frac{\left|\left|\nabla Z(x)\right|\right|}{2 \cdot Z(x)}\right)^2 = \left(d^T \cdot \frac{\nabla Z(x)}{\left|\left|\nabla Z(x)\right|\right|}\right)^2 \left(\frac{\left|\left|\nabla Z(x)\right|\right|}{2 \cdot Z(x)}\right)^2 = \left(d^T \cdot \frac{\nabla Z(x)}{2 \cdot Z(x)}\right)^2 \text{ ([7])} \qquad (6)$$

In the above formula, the $\cos(\theta)^2$ term represents the combination of specular and diffuse reflection, in which θ is the angle between the surface normal (displayed as semicircle or curvature in the two-dimensional ultrasound image) and the incident ultrasound radiation. The index value is set to 1 for a perfect diffuse reflection and any value larger than one for the combination of specular and diffuse reflection, we simply adopt two for our work to obtain a decent reflection visualization. The second term $\left(\frac{||\nabla Z(x)||}{2 \cdot Z(x)}\right)^2$ is derived from the Snell's Law, the parameter Z stands for the acoustic impedance for different tissues between the two adjacent pixels in the ultrasound image. This parameter can be achieved by interpolating pixels at the same corresponding locations of the binary mask and the original CT oblique slices. The term is deducted into the dot product of the unit vector and the gradient vector along the ultrasound wave traverse direction. This can be simplified into two dimensional as the acoustic impedance change.

Absorption: Absorption accounts for almost all (larger than 95%) the ultrasound attenuation in the soft tissue inside the human anatomy [59]. While the ultrasound wave is transmitting through the tissue, the energy will be absorbed by the surrounding tissue, thus the light intensity of the wave (measured in $dB \cdot cm^{-1}$) will be attenuated up to different extent. "The types of tissues and their pathological states are closely related to the ultrasound attenuation properties" [60, 61]. The tissues that are known to generate acoustic shadows in diagnostic ultrasound imaging process are bones, gas and calculi, where no echoes can be visualized to the lower border of the image, from the interface of the typical incident tissues. This will generate a shadow artifact in the ultrasound image, where the area at the bottom can be dimmed and even shown as entirely black area. On the corresponding images, pixels that are located below such structures are therefore "in shadow".

The ultrasound absorption can be mathematically represented by the exponential law as the equation below:

$$\frac{I}{I_0} = e^{-\beta x} \cong 10^{-\alpha * d * f/10} \quad (7)$$

in which f is the ultrasound wave frequency. The exponential expression is often normalized to unit length as $\alpha = -10 \cdot log_{10}(I/I_0)$ in Decibel per unit length. The parameter α is in a approximately proportional relationship with the ultrasound wave frequency ranging from 200 kHz to 100 MHz [62, 63]. Typical absorption coefficients for various medium are already known, based on the mask volume in the previous section, it is able to estimate the coefficients by the identification of the pixel along the ultrasound ray traversing path.

The absorption is then tracked throughout the entire propagation course of the ultrasound propagation. This process initializes an original light intensity at the ultrasound probe (which is located at the center of the upper edge to the ultrasound image), takes all the pixels along each ultrasound transmission column, calculate the portion of intensity from reflection and absorption computation. This portion is iteratively subtracted from the traversed light intensity and combined into a multiplication term as below:

$$I(x) = I_0 \cdot \prod_{0 \le i < x} \left(1 - \frac{I_{absorbed}}{I_i}(i, d)\right) \cdot \frac{I_{reflected}}{I_i} \quad (8)$$

Radial blur: "The radial blur effect produces the blurred image around a specific point in the image due to the movement of a moving camera. This effect is extensively used to simulate the radial scanning motion of an ultrasound transducer" [64]. The radial blur effect can be achieved

in two aspects: in radial direction, the light intensity attenuates exponentially; while in tangential direction, the gray values of the pixels are convoluted so that it will have a blurred effect to simulate the realistic inherent and coherent imaging of ultrasound machine.

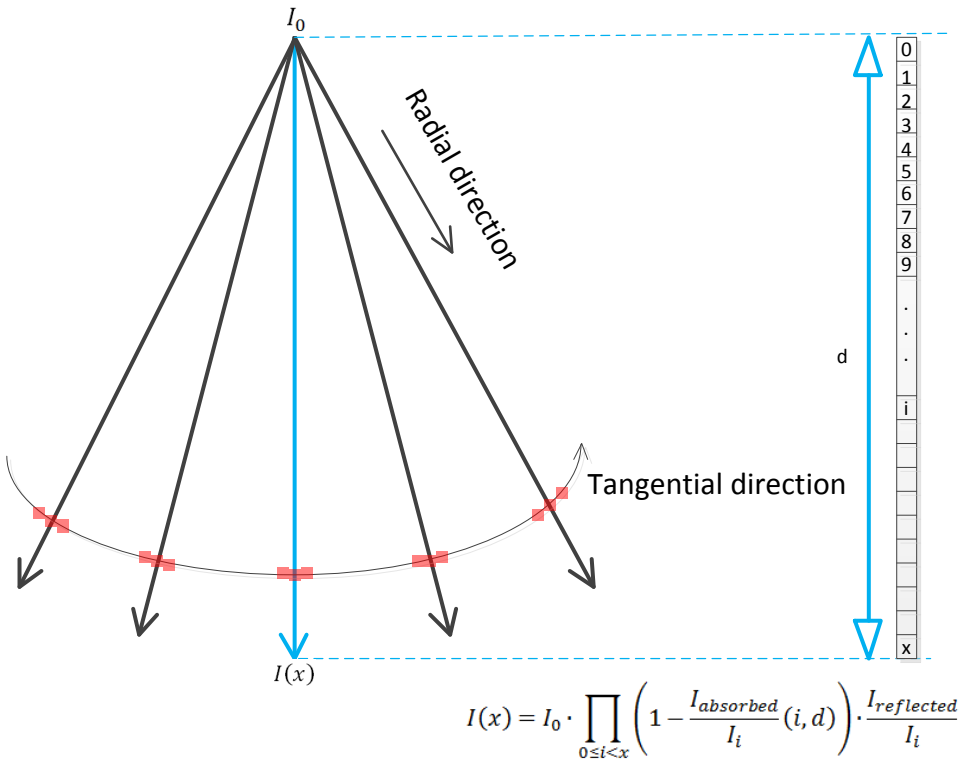

Figure 8. Demonstration of absorption and radial blur.

Speckle: A Perlin noise [65-67] pattern is designed and pre-computed onto the ultrasound image. Perlin noise is a function to generate coherent noise over a space [68], i.e., for any two points in spatial coordinate, the outcome of the noise function changes without continuities, as the point is moving from one next to another. The Perlin noise pattern applied within our work is applied on

two dimensional space and generate a noise texture that is overlaid onto the ultrasound image. The function can be represented by the function:

$$usnoise2d(x, y, p, r, t) = z \qquad (9)$$

The diagram below described the specific pipeline for generating noise value at the corresponding pixel location.

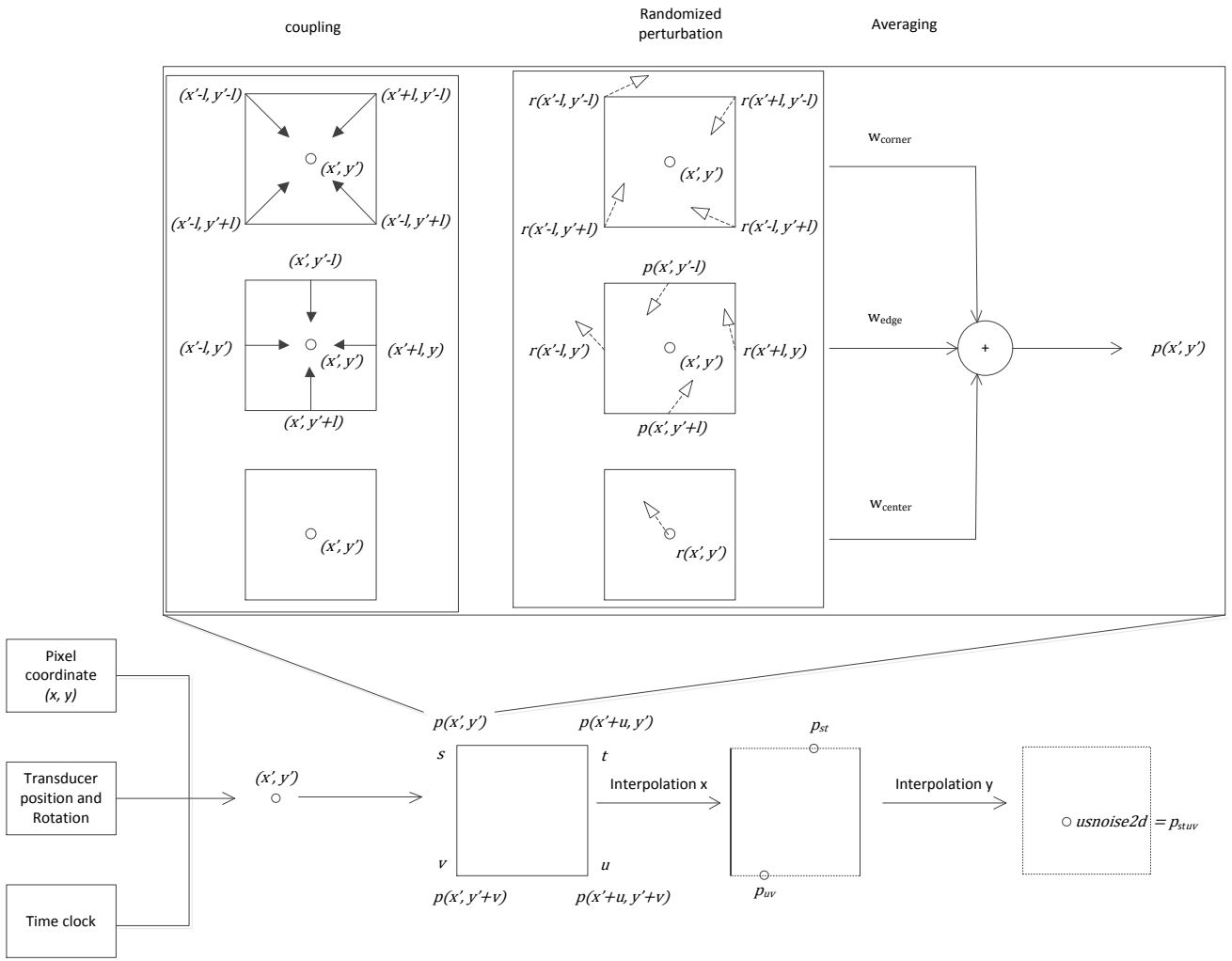

Figure 9. The pipeline of Perlin noise generation.

Since the noise texture is coherent with two dimensional coordinate ranging from 0 to 1, the seed of the pseudo noise generator is further related to the real-time transducer position, orientation, and the clock time to produce a dynamic texture in real time. The pipeline is divided into three steps: first, the coordinate value is combined with additional parameters and mapped onto a composite coordinate system, four neighbor vertices to the right and bottom sides are picked to calculate the randomized value. Next, each of the vertices goes through the same coupling and randomized perturbation steps. The outputs of the perturbation are interpolated on x and y direction respectively to compute the final Perlin value: usnoise2d.

Ultrasound mask: In order to guide a needle in interventional radiology, probes can be divided into linear, curvilinear and phased array types, based on the size and shape of their bottom face, i.e. “footprint” [69]:

1. Straight linear array probe: The crystal materials aligned at the flat bottom of the probe are aligned in a linear layout and generate round waves in straight line. The resulting image produced is hence in a rectangular shape. The linear probe generally has a higher frequencies ranging from 5 to 13 MHz that will facilitate the image in higher resolution with less penetration. This type of probe is suitable for ultrasound-guided procedures with imaging of superficial anatomical structures, such as central/peripheral vascular access, skin of soft tissue for abscess, musculoskeletal, etc.
2. Curvilinear array probe: Also known as convex shape probe. The curved bottom surface of the footprint will generate a fanning out shape of the beam. This structure produces the field of view (FOV) that has a much wider perspective. The curvilinear probe supports a lower frequency between 1 and 8 MHz, the deeper penetration allows for the

visualization of deep structure, at the expense of lower imagery resolutions. These probes are pervasively used in abdominal and pelvic procedures, as well as the evaluation of musculoskeletal procedures where deeper anatomy is necessary to be imaged from obese patient.

3. Phased array probe: The phased array probe has much higher density of crystals grouped closely at the footprint. It sends out oscillating sound waves originated from a single point and fan outwards, and creates a similar sector-type of beam image as curvilinear probe, though the probe has a smaller and flatter footprint than the curvilinear ones. The frequencies of phased array probe vary from 2 to 8 MHz. The smaller contact area determines that they are suitable for the procedure with maneuver at regions in small space, such as echocardiography or imaging between ribs in the flank or right upper quadrant.

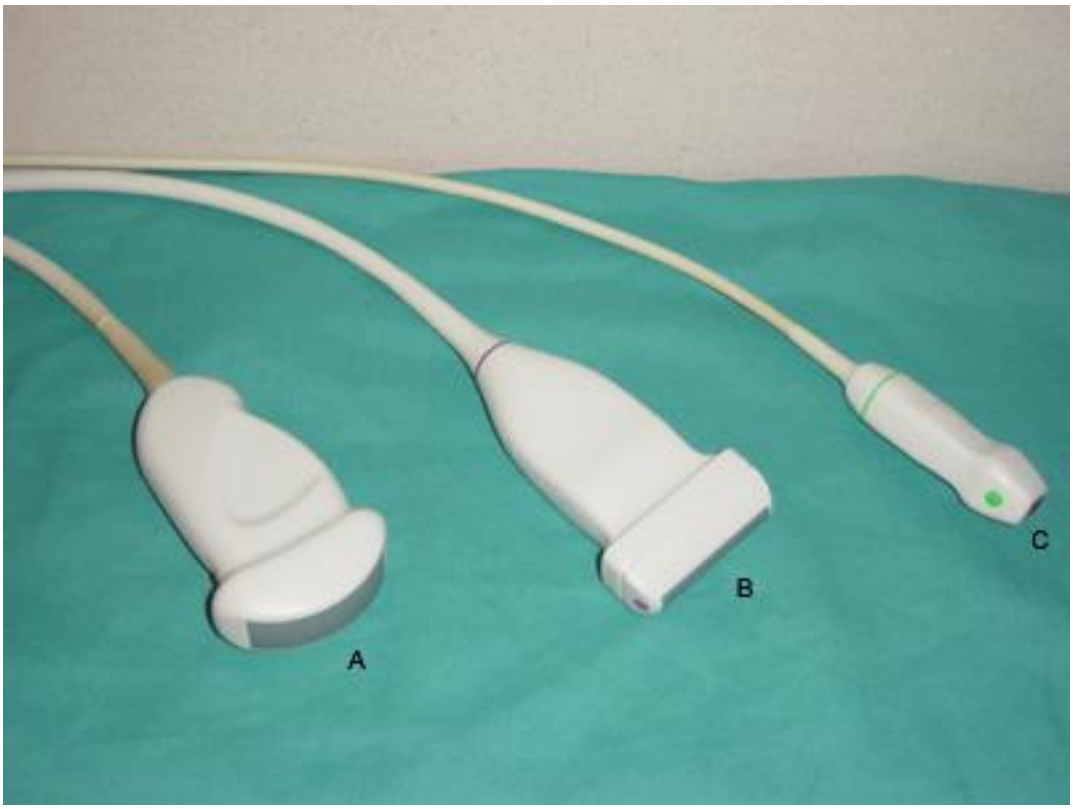

Figure 10**.** Different types of ultrasound transducers (A) curvilinear (B) linear (C) phased array**.**
(source: https://www.med-ed.virginia.edu/courses/rad/edus/technique2.html)

Using a linear probe produces a rectangle ultrasound image, while a curvilinear probe, the ultrasound image will reflect in a sector shape. In order to integrate this feature into the simulator, a field-of-view mask is calculated for the original 2D MPR image, the pixels that are within the mask region is assigned the pixel value at the position of the original image, and the pixels that are outside the mask region is given a black color, which stands for no information is available for the fragments within that area. The sector beam can be defined by three coefficients FOV angle α, inner radius r_1, and outer radius r_2, as shown in the picture below.

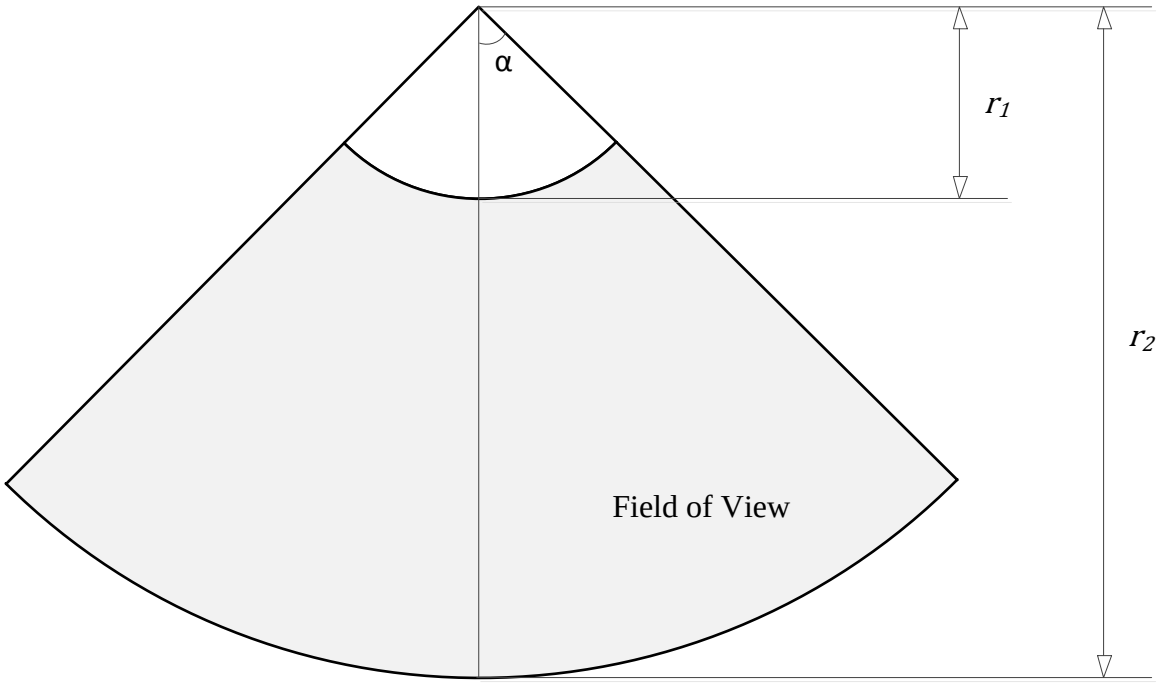

Figure 11. Ultrasound image mask for curvilinear probe.

In the above image, the parameter α determines the width of the horizon of the ultrasound image in polar coordinate, while the two distances are combined to decide the start and end distance of the depth that the beam is able to reach. The three parameters can be flexibly adjusted according to the real image that the ultrasound machine has generated in the conventional radiology operating room.

The Generation of Synthetic Ultrasound Image can be shown by the diagram as below:

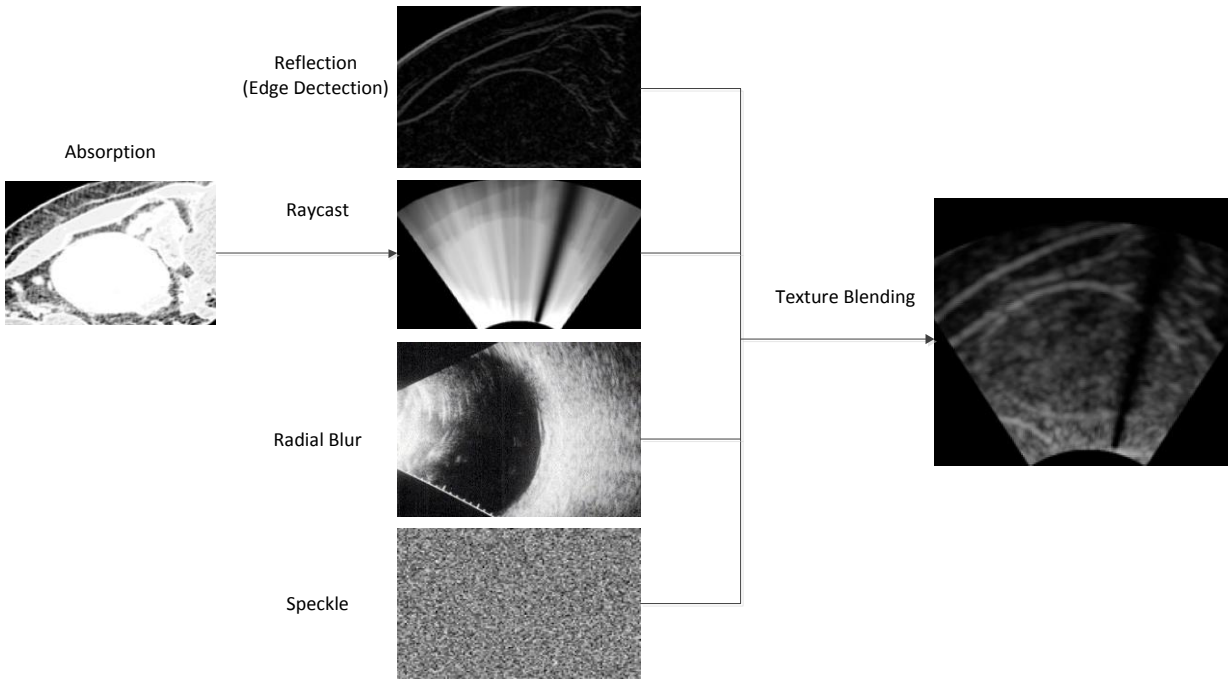

Figure 12. Synthetic ultrasound image generation using composite effect textures.

The four different effects are computed using two dimensional reformatted MPR images extracted from 3-D CT scanned volume. The features of reflection, raycast-based absorption, radial blur and noise pattern are then compounded as different independent textures and added in a post-processing step, producing a composite image in the real time based on the US transducer's interactive position to the virtual volume model.

Needle visualization

"The fundamental requirement for successful performance of US-guided procedures is needle visualization. The needle can be inserted by a landmark based approach or a freehand approach (the more challenging case within our work scope is when the user holds the transducer using one hand, while the other hand holds the needle unattached to the transducer, the coordination between the devices on both hands are necessary for the proper visualization of targeted anatomy, and the advancing course of the needle)" [70]. Although there are a number of commercially available needles designed to enhance needle visibility [11], the distinctive extent of the display of the needle under different surgical environments varies a lot. As the ability to visualize the needle during the central line placement procedure is the key factor of effective guidance to track the advancing course, the needle is attached to the combined image as an additional.

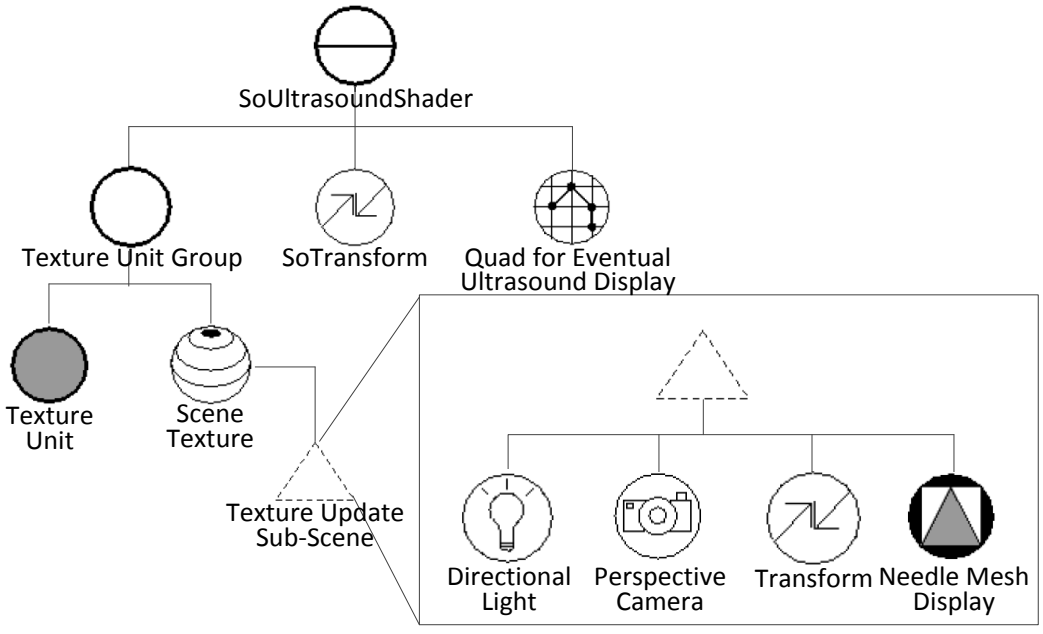

Figure 13. Scene graph of needle rendering.

Haptics Rendering

Preliminary

Haptics is related to the technique of incorporating touch and control into computer applications. “In order to create a realistic virtual or remote environment, precedence must be given to touch over all other senses because its perceptions have the most compelling character of reality” [71]. The artificial sensory information can be divided into two main categories as tactile feedback (also known as cutaneous information [72]) and kinesthetic force generation [73-75]. The former is formed from several modalities including pressure, object shape and curvature, vibration, temperature, pressure and local force. The latter is often related to force-perception or force-reflection. Haptic technology, which has proven success in the gaming industry [76], has shown great potential for the use in medical training, the high realism needed for effective surgical training, allows for little or no error makes the haptic-based simulators particularly attractive [77]. “Haptically-enabled medical simulations provide force feedback (sensing the resistance of pushing against virtual objects) and are based on sophisticated, high-fidelity haptic devices and software that deliver greater precision, differentiation between materials, such as bones and soft tissues, and a more realistic touch effects” [78].

There are common characteristics [79] to measure the performance capabilities of all haptic devices including:

1. Degrees of Freedom (DOF): “The set of independent displacements that specify the position of the end effectors”.

2. Workspace Volume: The area within which the joints of the device will permit the operator's motion.
3. Position Resolution: "Minimum detectable change in position possible within the workspace".
4. Continuous exertable force: "The maximum force that the controller can exert over an extended period of time".
5. Maximum exertable force/torque output: Maximum possible output of the device. Maximum force can only be exerted over a short period of time compared to the continuous force.
6. Stiffness: the touch sense of the surface of virtual objects, this is determined by the peak force/torque output, "but also related to the dynamic behavior of the device, sensor resolution, and the sampling period of the controlling computer".
7. Haptic update rate: The inverse of system latency in Hertz (Hz).
8. Inertia: Perceived mass of the device when in use.

A list of available generic haptic devices to be compared:

1. The PHANToM family of devices, developed by SensAble Technologies [80], which was acquired by 3D System Geomagic [81] on 2012,
2. The mantis Workstation by Mimic Technologies [82],
3. The Delta family and Omega.x family devices by Force Dimension [83],
4. The Falcon device by Novint Technologies [84].

All the above mentioned generic devices provide 6-DOF output, the movement of which can be freely tracked for movement and orientation. The PHANToM Desktop and Omni devices are

selected for the ultrasound guided needle insertion simulation, as they are well adapted to simulate the ultrasound transducer and needle.

Currently, the haptics rendering APIs [85] that support scene graph implementation are listed as:

1. Computer Haptic & Active Interfaces (CHAI 3D) [86]: "CHAI 3D is an open source set of C++ libraries originally developed by members of Stanford Artificial Intelligence Laboratory (SAIL) for computer haptics, visualization and interactive real-time simulation" [87]. CHAI 3D implements its proprietary collision detection mechanism, various haptic rendering techniques, etc. Based on GLSL, it also facilitates different functionalities as force shading, collisions computation between meshes and implicit functions, etc. However, even though it supports the scene graph and low-level communication layer implementation, it does not include any extra visual or sound effects. It is a suitable API for academic and research rather than for sophisticated applications, while the libraries can be extended conveniently. The API does not maintain an existing manual documentation, but the source code is very well reader friendly and easy to scan through.
2. H3D API [88]: H3D API is a high level open source scene graph library developed by SenseGraphics [89], it uses OpenGL for graphics rendering and X3D XML-based file format to represent the scene. The scene definition includes a set of XML nodes of light, camera, primitive objects, complex objects and textures, etc. On the low-level layer, it utilizes HAPI [76] for haptics rendering functionality. The H3D API provides interfaces for C++ and Python languages to parse and bind node definition in X3D in order to create scene objects and pursue better rendering performance.

3. OpenSceneGraph Haptic Library (osgHaptics) [90]: OpenSceneGraph is also an open source library developed at VRLab, Umea University. It is written in C++ and built upon OpenSceneGraph and OpenHaptics. Such that it integrates various rendering features from both libraries.
4. ReachIn API [91]: The Reachin API is a close source library developed by Reachin Technologies AB[92]. Rather than using Web XML script for initializing scene graph, the developed application relies upon VRML file format. It makes use of C++ and Python for computation optimization, and non-critical scripting tasks such as routing interface interaction events. The VRML nodes are used for describing and storing the 3D scene geometry. It allows for shading languages such as OpenGL Shading Language (GLSL) [93] and various haptic devices, such as 3DConnexion [94], SensAble [80] and Force Dimension [83] devices series, etc.
5. OpenHaptics SDK [95]: OpenHaptics is a commercial software development toolkit designed to work with SensAble devices ranging from low cost Omni to larger Premium series. The toolkit contains scene graph API for rapid development, it develops HD and HL API to support for integration both high and low level haptics into existing applications. Its latest version 3.0 includes the new QuickHaptics micro API [96], which enables rapid program design and deployment. It simplifies the process of adding kinesthetic feel of what users see and/or hear on the computer screen. Features include continuous monitoring the depth of penetration from surface contact point (SCP), various 3D model format support (3DS, OBJ, STL, PLY, etc.) to eliminate the need for format conversion and make individual adjustments to the torque parameters on 6DOF devices. OpenHaptics is also available in Academic Edition.

Dual Devices Haptic Effects Rendering

Two haptic devices are used concurrently for the simulation of the ultrasound guided central line placement procedure. Hence, separate haptic rendering contexts are created and generate forces for only one device. For the haptic device that manipulates the ultrasound probe, only the contact force rendering is required, as the probe only makes contact to the skin for palpation purpose and will remain on the surface of the human body anatomy. While for the needle that performs the invasive penetration procedure, various kinesthetic force generation is required for constraint rendering during the insertion through different percutaneous tissues. Three types of haptic effects are rendered for the needle:

1. *Viscous*: This effect is used to simulate the resistance arising from the friction between the needle shaft and different tissues, which is proportional to the velocity of the needle shaft during insertion course.
2. *Fulcrum*: This type of effect is extensively studied in the context of laparoscopic performance [97-99]. It is used to simulate the mechanical constraint at the incision point at which the needle is inserted during the surgical maneuver in the relatively short distance of the incision [100]. This effect allows the users to re-orient the needle when they realize that the needle is not in a correct track to approach the targeted region.
3. *Line*: The lateral movement and orientation of the needle starts to be restricted when the distance between the needle tip and incision point exceeds a threshold. This is used to gradually increase the difficulty of adjusting the needle direction as fulfilled in previous fulcrum effect, thus only the insertion movement along a straight line is allowed.

Table II
COLLISION DETECTION LOGIC TABLE

	Transducer	Needle	Haptic Skin	PhysX skin	Vein	Artery	Bone
Transducer	-	○	×	○	×	×	×
Needle	○	-	○	×	○	○	○

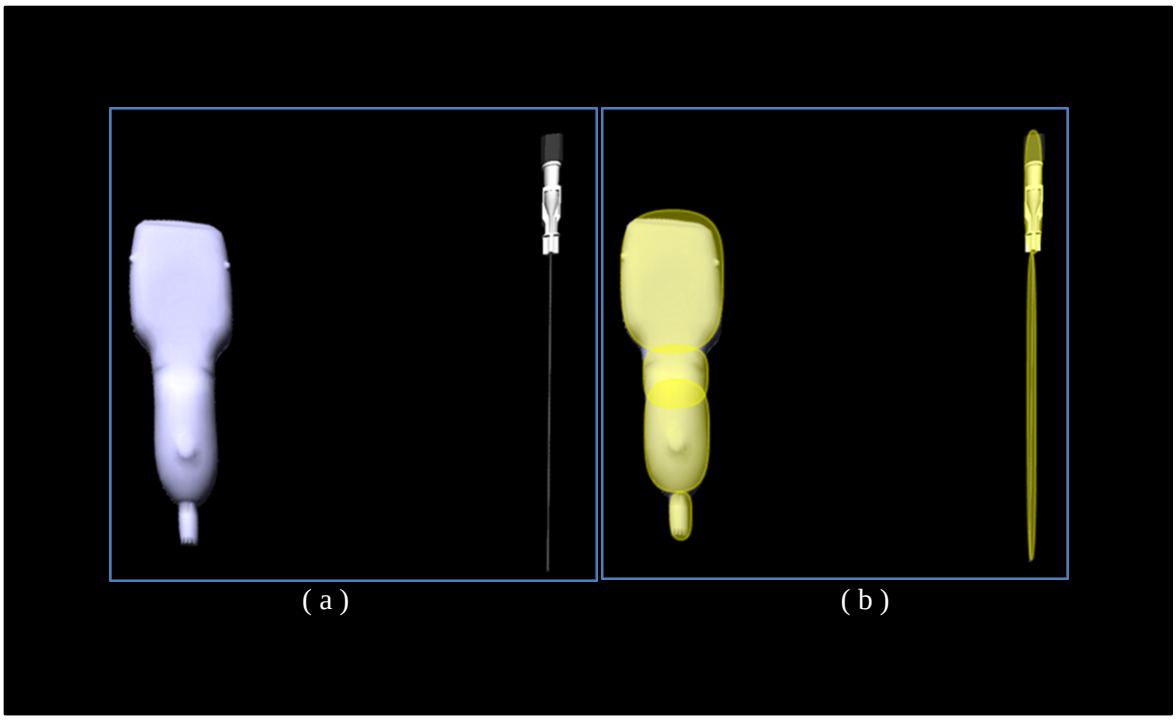

Figure 14. Capsule representation for ultrasound transducer and needle.

The geometry of ultrasound transducer and the needle are triangular meshes, the collision detection between which are relatively expensive. A set of invisible bounding capsules are overlaid on the object geometry of ultrasound transducer and needle to prevent the mutual penetration between the two proxy shapes. The collision detection between capsules is very fast and robust, and is therefore a great choice to approximate shapes with round surfaces.

Results

Central Line Venous Catheterization Procedure

The developed algorithm is incorporated into a VR based immersive environment, where the graphics and haptics threads run at different frame rates. The resulting image, as well as the volumetric display, is demonstrated.

The specific steps to perform the CVC training simulation procedure are as follows:

1. To begin the procedure, an optimal position of the patient is determined. The virtual model of the patient is placed at multiple different supine, in most cases Trendelenburg positions. These preset transforms are determined based on the collected evaluation comments from group of participant surgeons of which they think are the most comfortable to carry out the training procedure. Users are able to switch between different pre-defined positions by pressing specific keyboard button, or manually customizing the position by holding haptic device button and rotating the patient model.
2. Palpate the patient by manipulating the transducer and identify the insertion site. Position the transducer so that the internal jugular vein is centered in the resulting ultrasound image, where the transducer is being placed between the two heads of sternocleidomastoid muscle. Apply the force while contacting the neck landmark area to observe the collapse of the vein, obtain a best insertion location where the vein can have the largest exposure on the ultrasound image.
3. Use a gauge needle to puncture the skin at the center of the transducer maintaining a 45° angle from the transducer. The needle can be inserted at the perpendicular direction to the

transducer, rendering a cross-sectional view in the ultrasound image, or to the parallel of the ultrasound probe footprint plane, and observed as longitudinal view. Use the ultrasound image to trace the advancing path of the needle. To make sure the needle is in the correct advancing track towards the targeted area, use the technique of tilting the transducer back-and-forth or by withdrawing the needle and realigning it.

4. When the needle has successfully penetrated into the vein, a highlighted color indicator on the needle will be displayed and the metrics on the simulation screen will be updated. Try to prevent the inadvertent vascular punctures into the carotid artery or the posterior wall of the vein that are prone to cause complications.
5. Once the trainee has established a successful access into the vein, the relative position and orientation of needle with respect to the anatomy are frozen, and the volume of the patient anatomy is clipped away while being tilted to examine the exact location of the needle. This can be done using the peripheral foot pedal of the simulator.
6. Upon the success or failure of the insertion, the needle needs to be pulled back and the insertion direction needs to be realigned. If the needle is entirely removed from the skin, a highlighted color is displayed on the top of the needle, make sure to replace for a new needle by touching the reset button on the upper right side of the simulation interface, this will reset the needle color indicator as well.

A detailed pipeline of the procedure simulation is depicted in the flowchart below:

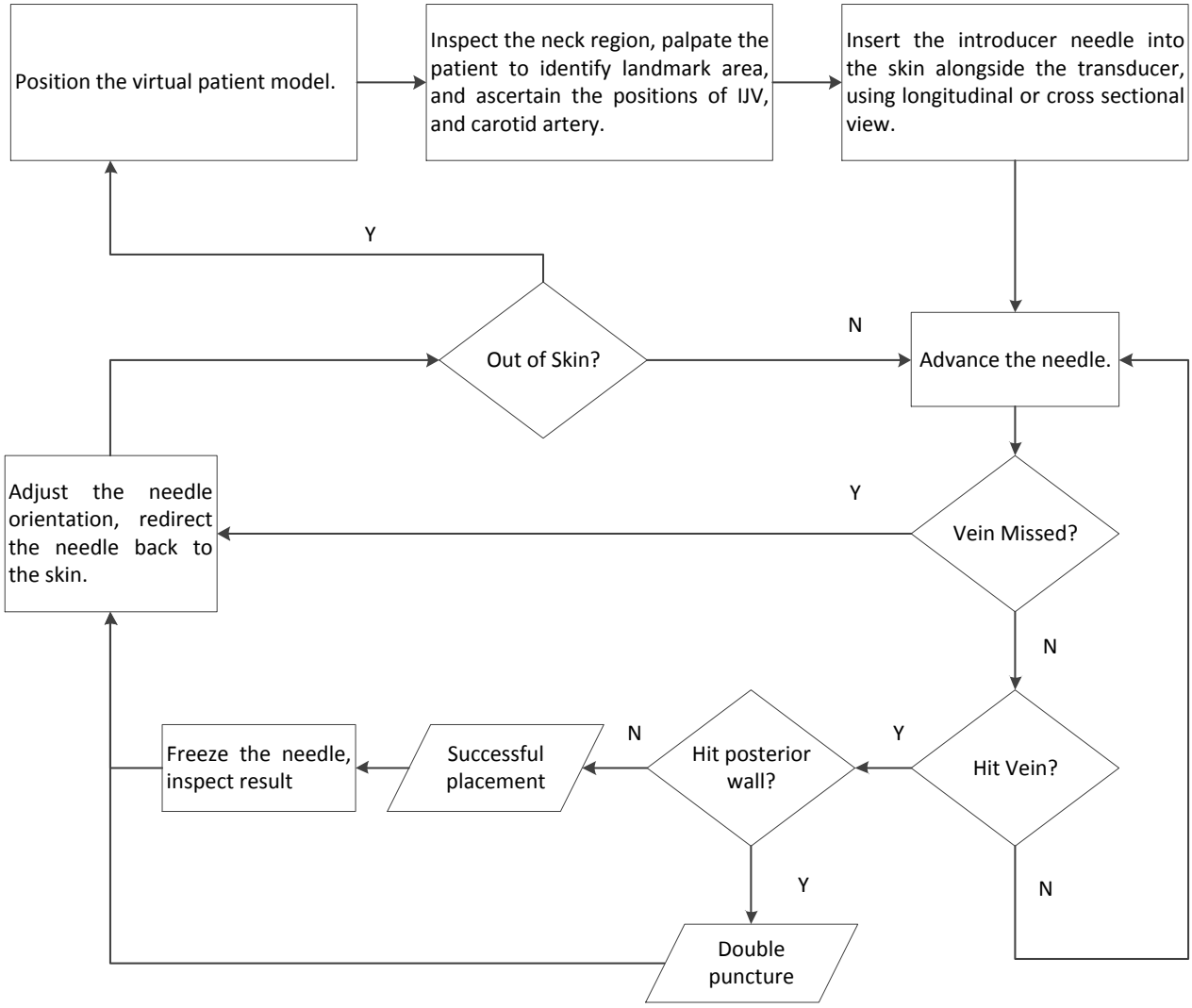

Figure 15. Central line placement training procedural steps.

Simulation Environment

The CVC application runs in an immersive augmented reality and haptic simulator known as ImmersiveTouch® [101]. The simulator is responsible for the stereoscopic rendering and user operation interface (i.e. head tracking, haptic input by hand), and ultrasound image display.

As for the volume rendering, a CUDA based enhanced marching cubes algorithm is implemented to improve the surface features of the volumetric meshes, and thus, remarkably improve the quality of the haptic interaction. OpenHaptics based haptic effects are rendered for the collision tactile feedback between the instruments and different isosurfaces such as the veins, arteries, and bones.

Deformation Demonstration

Before the catheterization procedure takes place, an ultrasound transducer manipulated by one SensAble® Phantom device is placed on the surface of the neck to assess the position and the appearance of the internal jugular vein and carotid artery next to it (cf. Fig. 16). Based on the collision detection algorithm and a spring-damper model, a haptic library is utilized to render the local deformation on the contact point between the instruments and the skin, without affecting the haptic performance [101]. Figure 8 shows the ultrasound image in a cross sectional view of the vein.

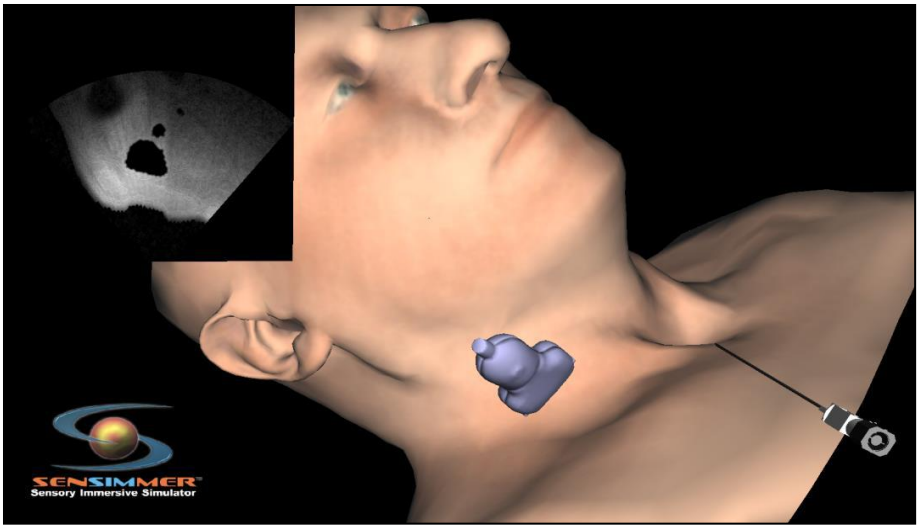

Figure 16. Locating the vein using ultrasound.

In the visualization, the IJ vein is compressible compared to the carotid artery, which is not compressible. Size and location of the vessels are highly variable and cannot be used to determine which vessel is the vein. By applying a small amount of force on the skin, the vein will display the characteristic compression. Figure 9 shows both the original uncompressed vein (in smaller circles) as well as the compressed vein (in larger circles), as the result of the pressure applied by the transducer (compare the vein to the artery). The ultrasound can be viewed at any axial plane according to the position and orientation of the transducer. Figure 10 shows a cross sectional view of the neck.

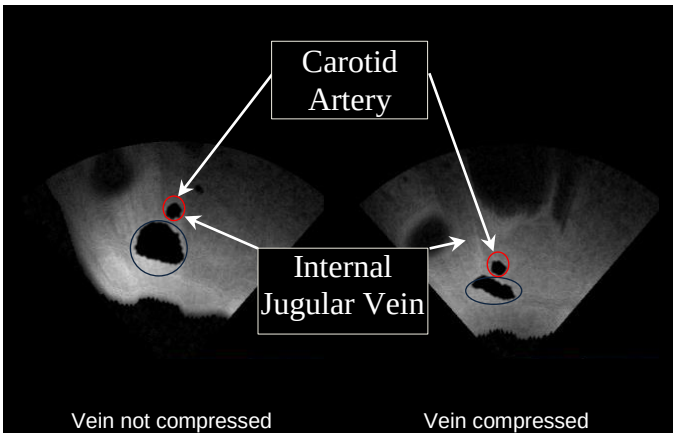

Figure 17. Simulation of vein compression.

Depending on different standardized positioning of the transducer, the vessels will have different interpretation in the resulting image. Different alignment of the needle will also affect the portion of the needle displayed in the ultrasound image. When the needle is inserted perpendicular to the ultrasound beam (cf. Fig.18), only a portion of the needle is visualized, while in a parallel alignment (cf. Fig.19), the entire course of the needle can be visualized during the traversal.

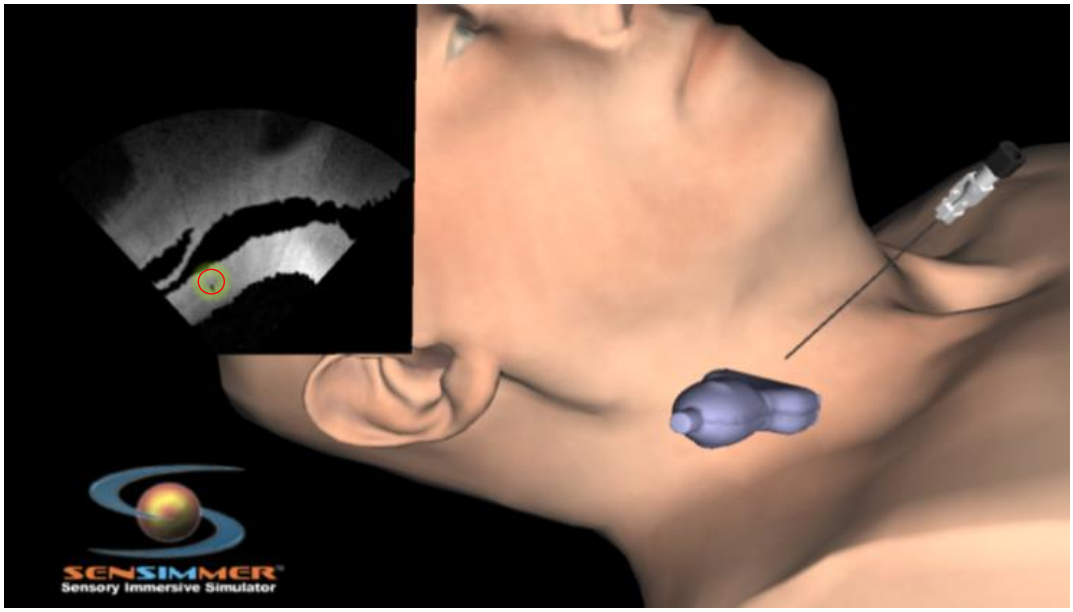

Figure 18. Needle insertion in longitudinal view of the vein.

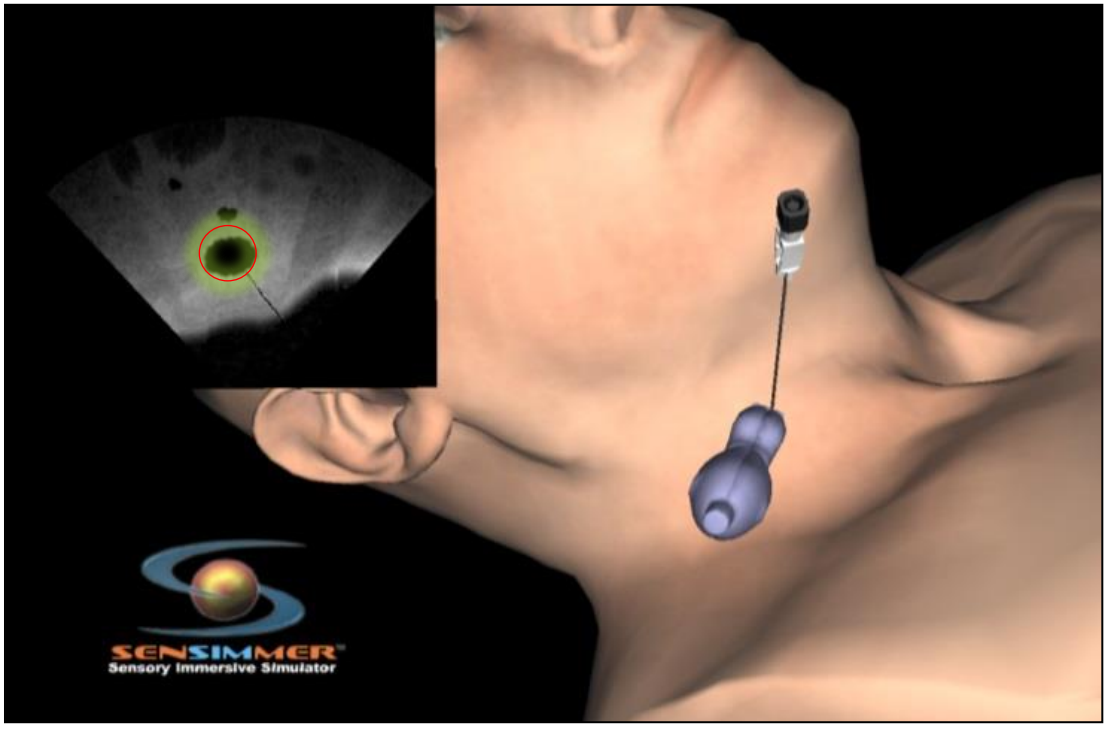

Figure 19. Needle insertion in cross-sectional view of the vein.

After the targeted placement spot is determined, a virtual needle, controlled by another Phantom Desktop haptic device, is inserted into the virtual patient. The ultrasound image shows a portion of the needle approaching the vein (cf. Fig. 20).

Once the needle has been placed (hopefully in the vein), the trainee can reduce the transparency of the skin and rotate the virtual model of the patient to assess the relative position of the needle and the vessel from any 3D perspective.

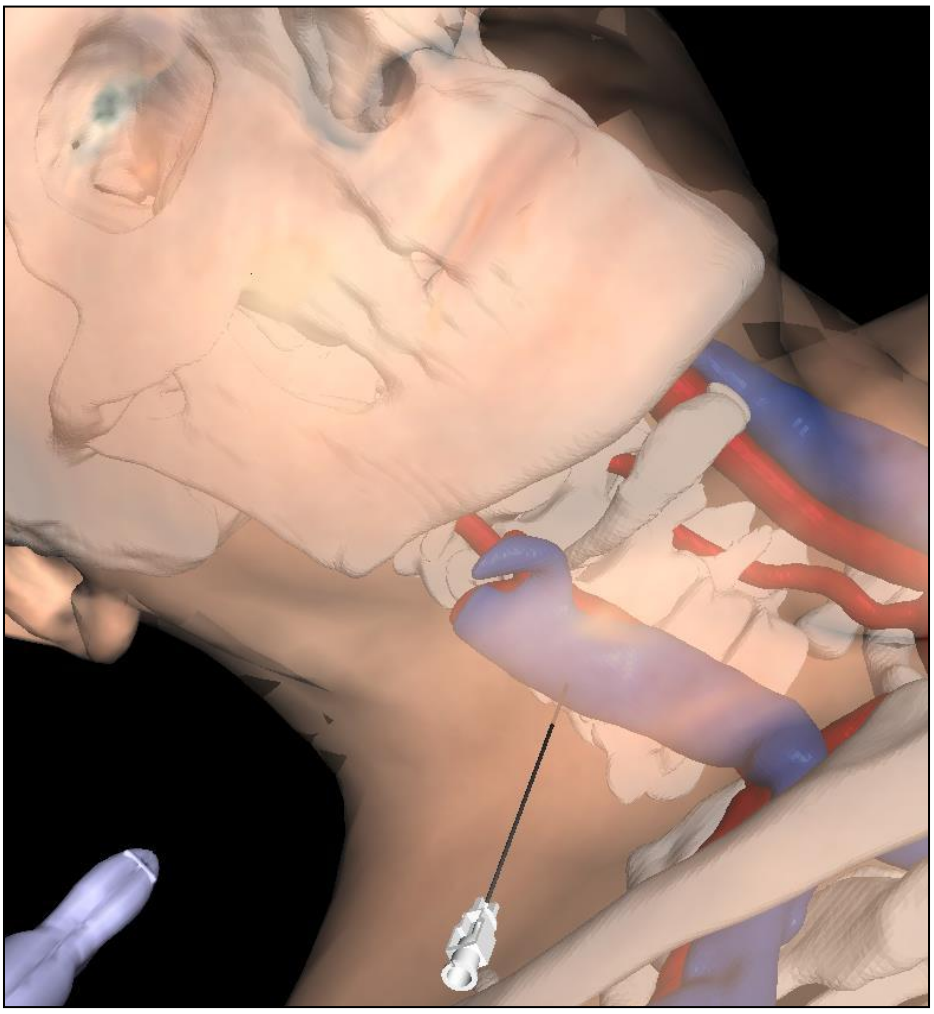

Figure 20. Needle position verification through transparent skin.

Procedural Performance Evaluation Design

Performance Data Collection System

The ultrasound program is further integrated into the multi-discipline curriculum environment. The curriculum system serves as a hub of the entire procedure sets that are taught to the residents. The trainee information, as well as the operation performance statistics is recorded during the run time of the simulation and stored into the background database system. According to the overall performance, the next level of the training procedure will be activated and that the students are guided to perform and complete the whole curriculum. On the other hand, the instructor who has the administrator's privilege is able to see the statistic base off of the entire class and select the profile of specific student to analyze and improve the teaching. The curriculum system provides an integral framework to test the collect the feedback from the universal users at different locations. A screenshot of the curriculum web interface for user performance management is shown as below.

Figure 21. The multi-discipline curriculum system interface.

Indicators on the needle for post catheterization procedure

The importance of ultrasound guided intervention procedure is not limited to the precise identification of the various tissue structures in real time. A comprehensive training system would also require a validation mechanism to assess the clinic success. As for the internal jugular approach of central line placement, after the catheter is placed at the ideal target inside the carotid vein, the color and pulsatility of the blood can be a useful indicator to determine whether the central line catheter has been properly placed. This is a crucial phase to finalize the training procedure from a surgical perspective, and increase the reliability of the program to lay down the statistics of the successful puncture.

During the simulation, it is important for the user to know the specific status of the needle during the advancing course. Clinically, once the needle is inserted into the lumina of the vein, the negative pressure inside the syringe that is connected to the needle will suction the blood. While the non-pulsatile blood is a positive indicator of successful arterial puncture, the pulsatile blood flow in bright red color is suggestive of arterial puncture. In the real-time simulation, this status is indicated by the color change on the needle shaft. The needle will turn into green color after successfully puncturing the vein, while it will turn into red if the event of puncturing wrong area is detected. Among the multiple attempts of insertion, it might be occasionally the case that the needle needs to be withdrawn completely out of the skin and reinserted again using a replaced new needle. This replacement step is mandatory for sterile purpose that a yellow indicator is highlighted every time the needle is pulled out. This indicator will be reset only when the user performs an additional step before reinserting by contacting a toolkit object in the scene, representing the replacement.

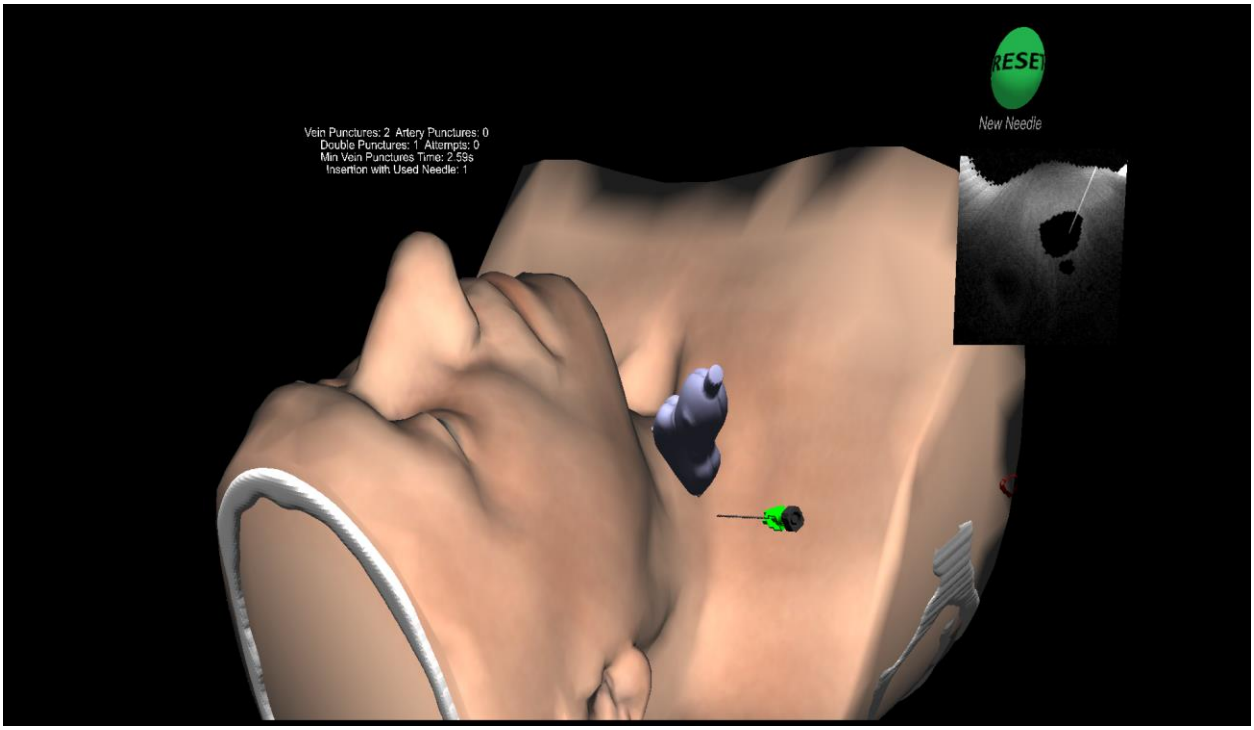

Figure 22. A green indicator on the needle top indicates the correct placement into the artery.

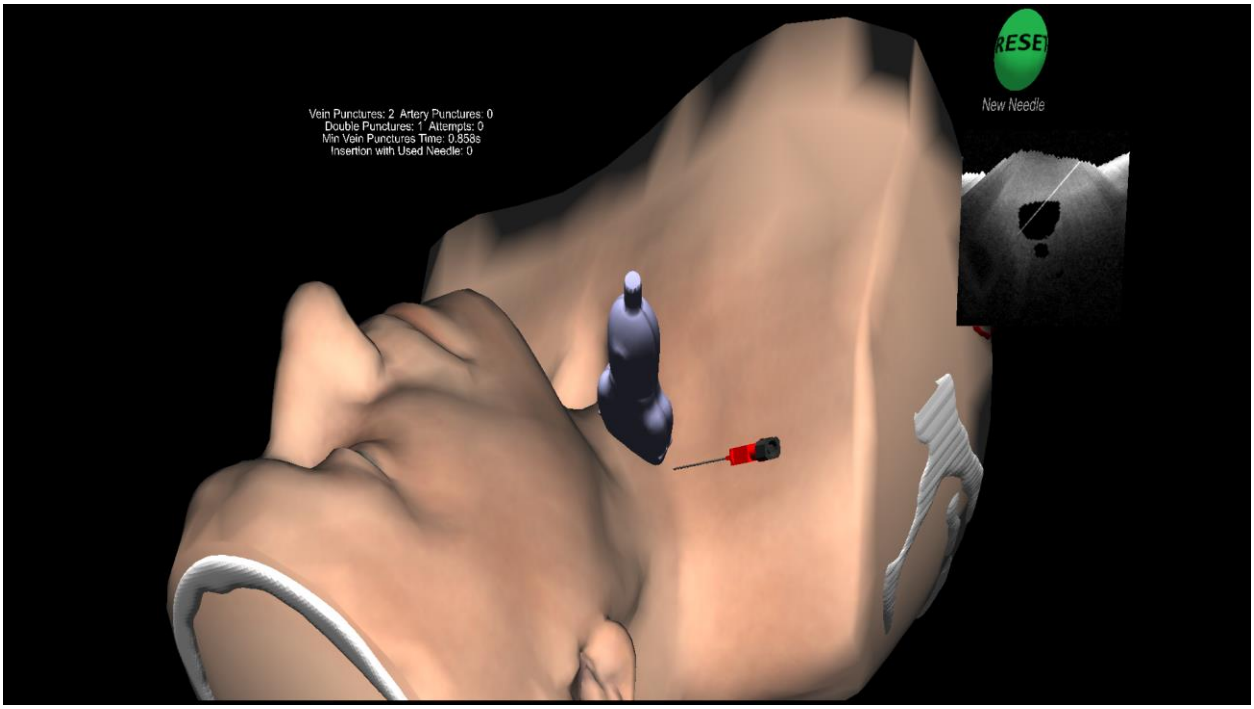

Figure 23. A red highlighted color on the needle top indicates the occurrence of complications.

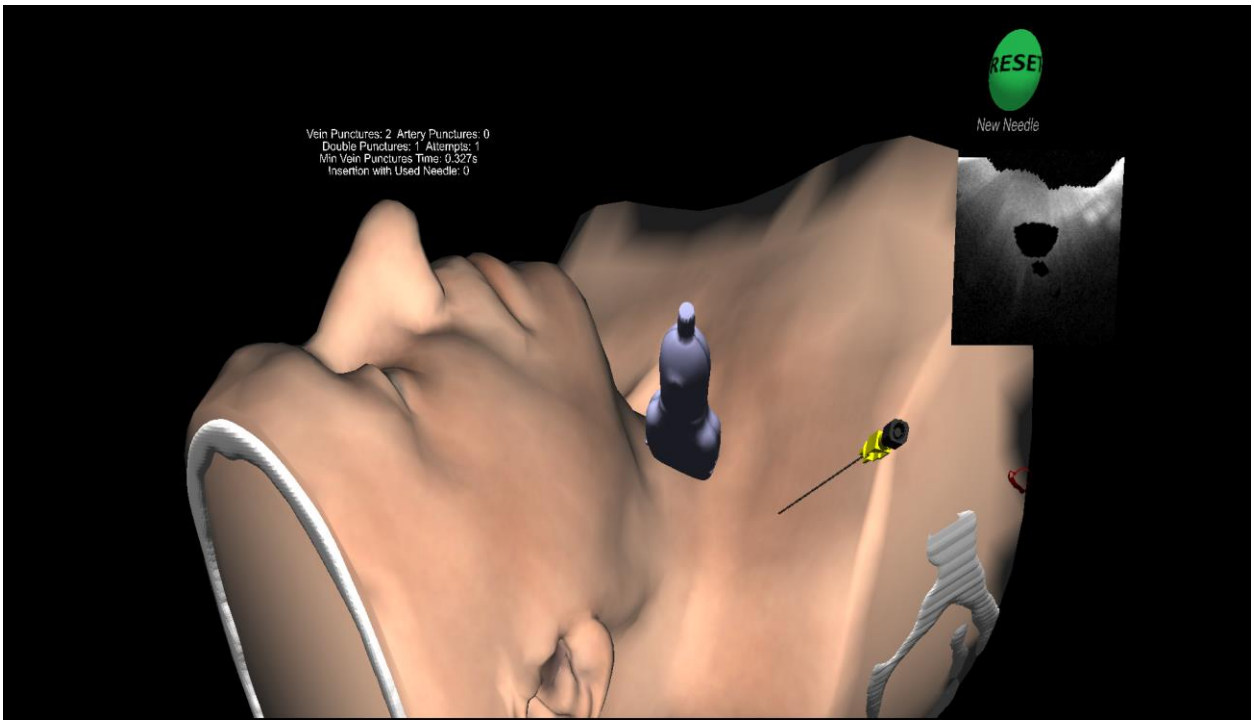

Figure 24. A yellow highlighted color indicates the needle needs to be replaced.

Implementation of Performance Metrics

A set of break-down measurements of operation performance on the simulator is designed to help the trainee identify the dangerous or inadvertent operations that potentially cause any intermediate or delayed complications. These standardized metrics are saved to the background database every time the trainee presses the pedal to freeze the needle. The metrics data is useful regarding the recognition of the incorrect operation in real-time by prompting the metrics on the Graphic User Interface, simplifying the case for the instructor to teach the right technique to place the needle, which effectively reduces the incidence of central-line associated bloodstream infections (CLABSIs) [102, 103]. The occurrence of pneumothorax is considered to be higher with the subclavian vein catheterization, and "the risk of pneumothorax can be minimized by the use of ultrasound guidance" [104]. Thus, this metric can be added into the curriculum upon further educational requirement. The metrics can also be further compiled as quantitative evidence to the users' progress on overall learning curve.

The types of metrics are essentially the statistics of the incidents that indicates the effective insertion, the sophistication of the trainee on the procedure, and more importantly, the behaviors closely related to the majority of mechanical complications of CVC applications. According to a reportable series [105-107] on the complications rates of central venous access approaches, the most significant causes are vascular injuries [108], as well as accidental puncture or laceration. The purpose of the metrics is used to enhance the users' performance and avoid the vascular injuries that are prone to result in the subsequent frequently occurred complications including arterial puncture (6.3-9.1%), thrombosis (7.6%) and hematoma (<0.1-2.2%).

It has also been shown from multiple studies that the rates of local or systemic infection can be reduced with the use of maximal sterile-barrier precautions, including the sterilization of mask, cap, gown, and large instrument. Also the practitioners or residents are recommended replacing the needle after removal from each insertion attempt to prevent the cases of venous air embolism or infections caused by the bacteria, viruses or fungi via the improper contact between the needle shaft and insertion site area.

The performance metrics used to assess the training results can be described as follows:

1. Number of times of vein punctures: Measures the total number of attempts that the needle tip is successfully inserted and placed into the blood lumen of targeted vein.
2. Number of times of artery punctures: “The traditional method for avoiding the placement into arterial vessels is to concentrate on the color and pulsatility of blood coming from the needle hub, which has been reportedly regarded as unreliable. A hematoma at the insertion site can highly likely occur particularly if the carotid artery is punctured by mistake” [109-112]. The incident of mistakenly artery puncture can be recorded with ultrasound guidance within which the needle is accurately aligned with the volumetric anatomy model in real time.
3. Number of times of double punctures: During the central venous access procedure, the needle should be inserted slowly enough to prevent that it entirely went through the vein, with the assistance of ultrasound. This malposition rate of the needle has been reported as high as 64% from the participating residents who penetrated through the posterior wall of the internal jugular vein, according to a study in 2009 [113].

4. Minimum amount of time of vein puncture: The amount of time duration from the initial needle tip invasion at the wound site to the first-time penetration into the vein within one single attempt. This duration does not include palpation time using ultrasound probe prior to the needle insertion. This score is used to assess the efficiency of the trainee carrying out the procedure.
5. Number of times of insertion with used needle: For sterile purpose of the whole procedure, the trainees are requested to replace the needle, when it is pulled out of the skin after one particular time of insertion. Neglecting the replacement of the needle is considered as missing highly important sterile technique that is prone to cause the resulting complications.

The abovementioned five metrics are displayed as a group of scores in the graphic user interface (GUI). The break-down metrics are dynamically updated while the participants are interacting with the virtual patient's volume. By pressing peripheral foot pedal during the simulation, the metrics sets are updated into the background database, and further serve as the overall evaluation of the users' performance. Through the sequential training performance records, "the psychomotor skill transferability can be properly demonstrated by comparison of improvement of the trainees who use the simulator over those who do not" [114].

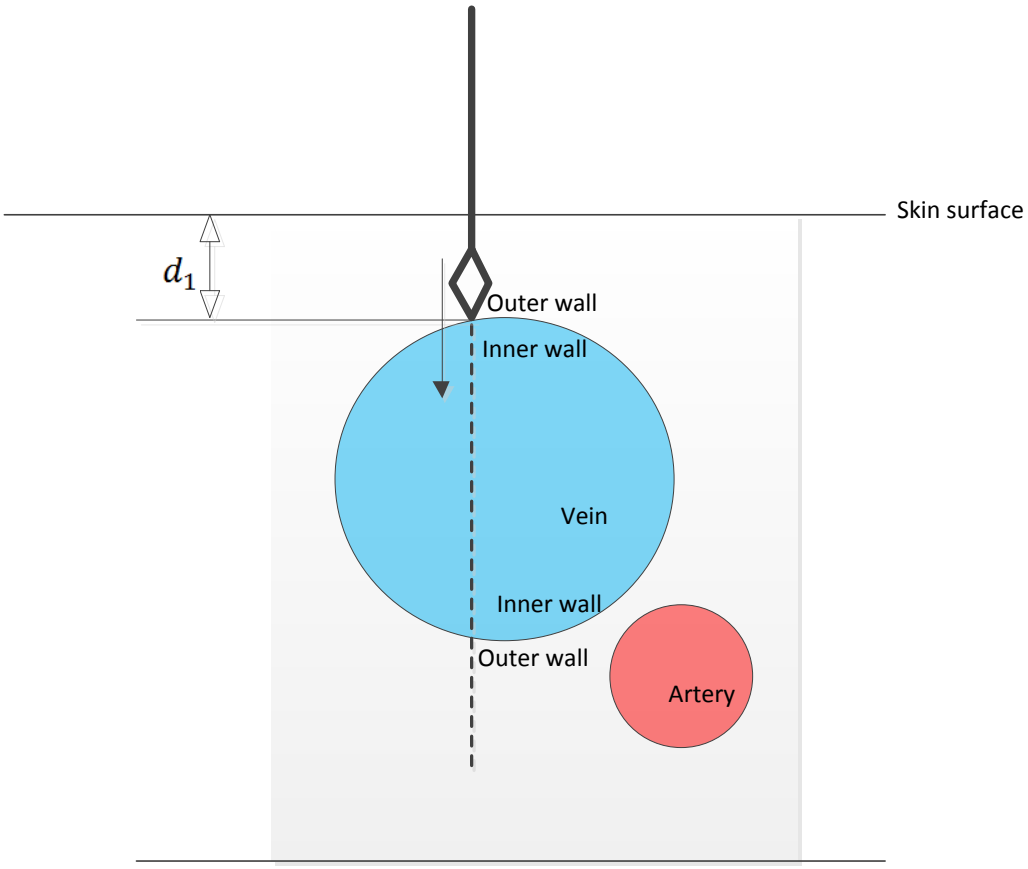

Figure 25. Advancing needle initially punctures the anterior wall of the vein.

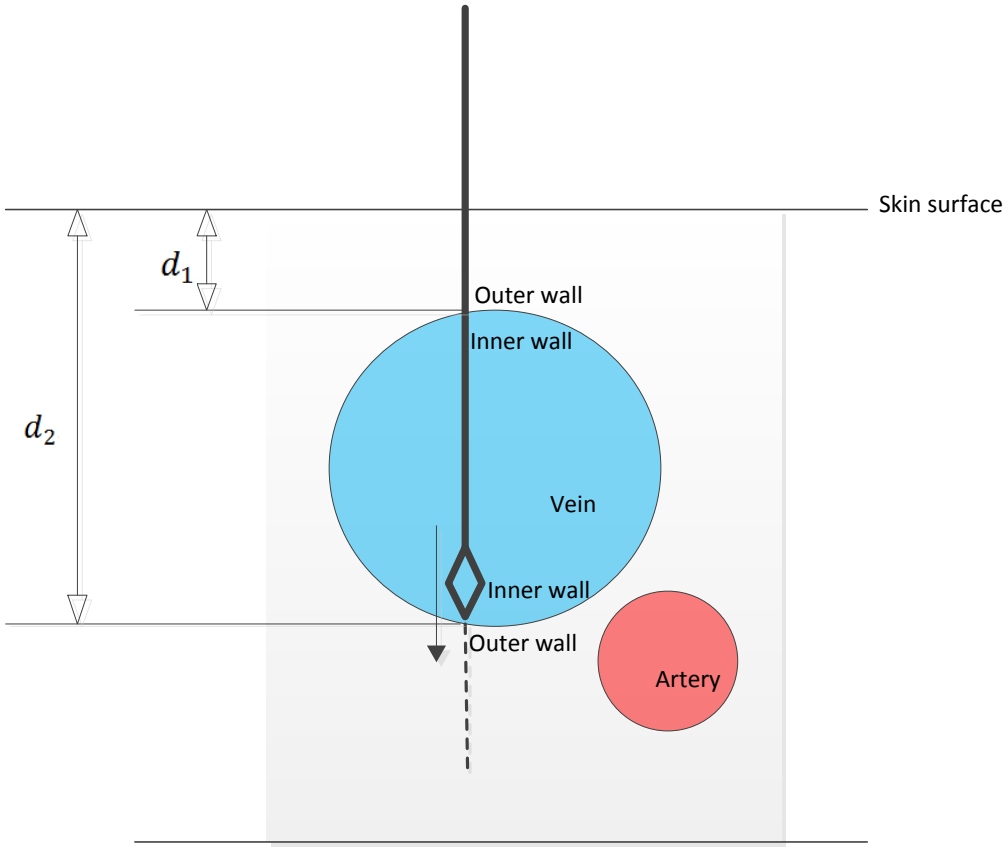

Figure 26. Advancing needle punctures the posterior wall of the vein, causing a double puncture.

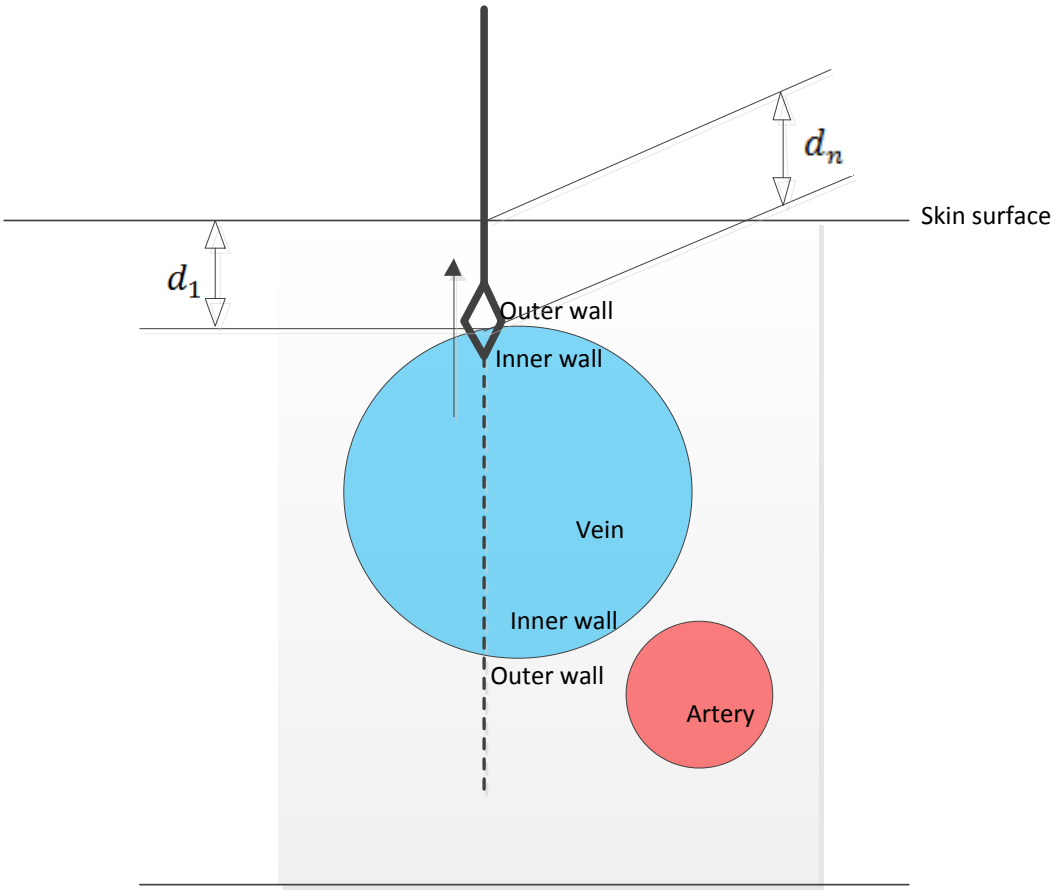

Figure 27. The retreating needle tip hits the original intruding site

During the advancing of the needle, it is important to record the advancing path of the needle, and generate the two distance parameters are maintained to track the depth of the needle under the skin. While the needle initially punctures and penetrates through the outer wall of the vein, parameter d_1 is assigned as the initial inserting distance from the wound point on the skin and the initial contact point of the vein. This parameter is necessary to detect the specific status of the needle when it hits the vessel wall for the second time: whether it pertains to the advancing event until it reaches the inner wall of the vein in the other end, or withdrawing the needle upon the

successful insertion. The needle insertion depth is being constantly recorded to compare with d_1: if the depth value is larger than d_1, it means the needle has hit the back end of the vein and cause a double puncture complication; while if the depth is equal to d_1, it indicates the needle is pulling out of the vein after a successful puncture.

Conclusions and Future Work

Contributions

As medical simulators are increasingly accepted as the alternative tool for experiential training systems, the training on a virtual patient rather than a plastic mannequin or cadaver may serve a great impact on the medical apprenticeship training. A virtual reality based simulator is dedicated to provide highly realistic replication of human physiology and extended anatomical variability. It facilitates the training of practitioners or medical residents on a virtual patient while collecting the critical analytics and feedbacks in a more systematic way, which can be used as an effective measure to consolidate skills to pursue higher proficiency on the procedure, and hence avoid drawbacks in the operation and guarantee the success rate while performing on the real patient. The ImmersiveTouch simulator has demonstrated this hypothesis by combining flexible components (realistic graphics display, high resolution haptics feedback, immersive training environment and various equipment input) for an integral simulation, while maintain a high profile performance.

The thesis work is developed on the resulting simulator further demonstrated the feasibility of the applicable application that utilizes off-the-shelf components to produce a start-of-art training environment. The contributions of this thesis work through Chapter 2 to 5 can be summarized in the diagram below:

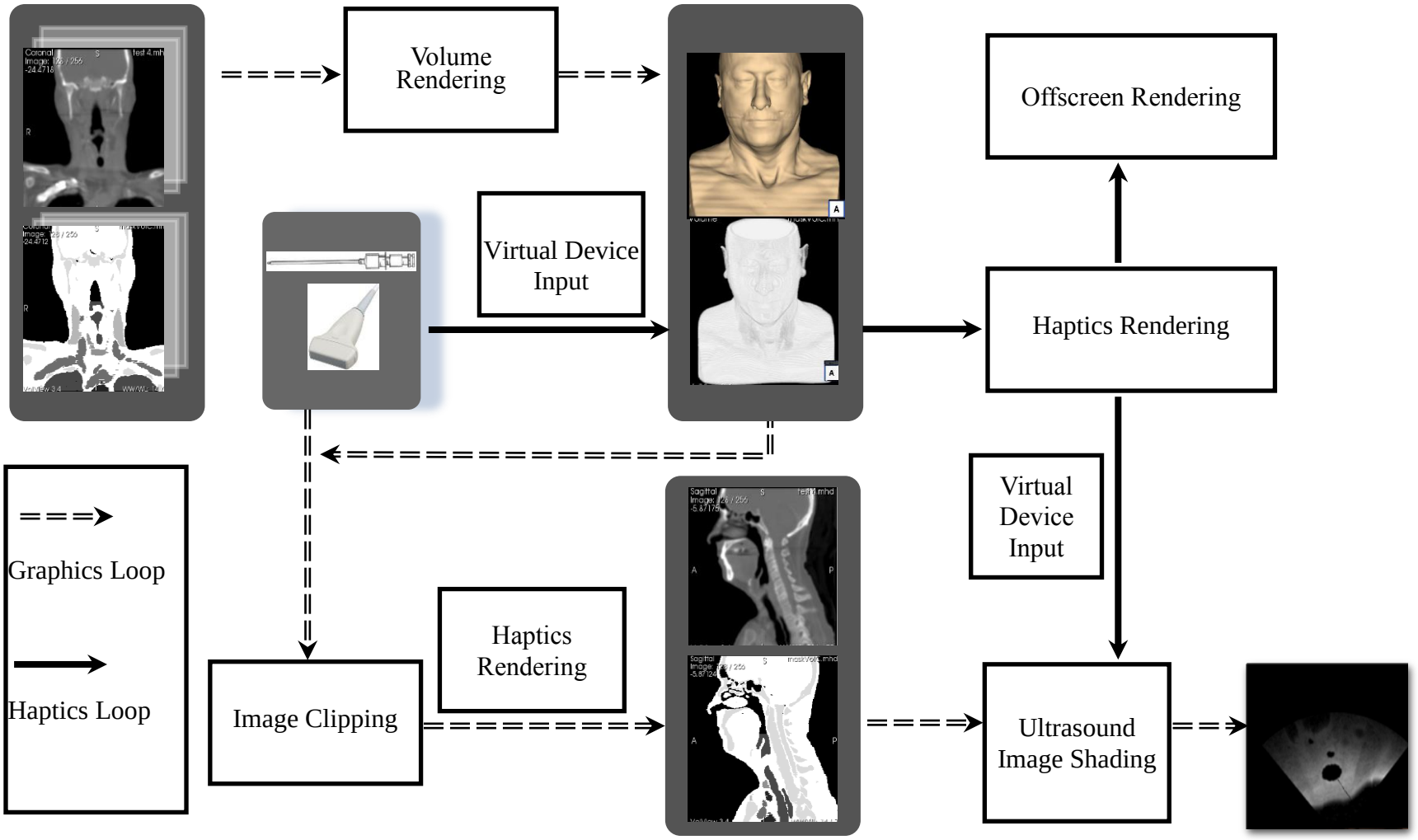

Figure 28. Central line placement diagram

The research work carried out respectively on the two main aspects of the simulation, i.e., graphics and haptics ends, includes:

1. Central line patient volume rendering: the original volume obtained from CT scanner is usually in a very high resolution, and is therefore overwhelmingly expensive to render in real time. On the other hand, the modality of CT is far from satisfactory in identifying the muscle and soft tissue in the subcutaneous area under the skin. Therefore, the resampling the consecutive oblique slices and cropping of the volume is necessary to obtain a dataset that will not exceed the memory limit of the simulator, while maintaining a satisfactory resolution. The CUDA Marching Cubes GPU based surface generation algorithm is involved and the surface smoothing is undertaken to generate an accurate yet cost effective performance. The manual segmentation of the volume is helpful of identifying the type of tissues with the pre assigned labels. With the accurate label information of the specific anatomical structures. A precise estimation of acoustic impedance as well as the elasticity properties can be obtained for interactive deformation computation. This approach has solved the inaccuracy caused by the interpolation which is error prone, while producing a feasible solution by GPU acceleration structure.
2. Tissue deformation effect in two-dimensional image: simulating interventional radiology imagery in real time is a challenging task as it needs the interaction between the anatomy and equipment for minimal invasion. Deformation of the vessels in central line placement using ultrasound guidance is the critical factor for the pre-surgical planning. In this work, a mass-spring system is designed compared to the other approaches, which is demonstrated to be a realistic yet computationally achievable solution. Only the voxels

within the two dimensional beam plane casted by the ultrasound transducer are taken into account, and ray-casting based force transmission calculation is carried out to simulate the collapsing effect of the vessels. Hitherto, none of such simulation is observed in other publications for the experiential training purposes.

3. Ultrasound effect computation: Trans-modality on-line ultrasound image is produced using the CT scan dataset, based on the position of haptic proxy in the virtual environment. Composite features observed in the ultrasound image are implemented using multi-texture technique by the GLSL implemented within the scene graph structure.
4. High resolution haptic effects: Haptic model for the ultrasound transducer and the needle were developed based on OpenHaptics. A realistic feedback to the haptic stylus as the operator is performing the procedure is the most important factor to promote the psychomotor skills of the trainee. Different types of scenarios of needle access to the bones, vessels and tissues are fine-tuned including viscosity, fulcrum and line effects. While the ultrasound transducer has been modeled as a contact type as it will constantly remain on the surface of the skin. The effects are rendered on both hands respectively to facilitate the real-time coordination of dual hand devices to carry out the free hand approach of central line placement procedure.
5. Quantitative performance recording: The automatic recording of the designated task while avoiding the inadvertent mal-operation provides an intuitive guideline while the metrics are dynamically updated in the simulation interface. With sufficient of the instructor guidance information, the instructor’s presence and intervention can be minimized. This metrics data over the entire training group can be saved and assessed

later for the learning performance evaluation of the users. And the user is able to see the visualized break-down result upon their further requirement.

Discussion and Future Work

During the initial pilot studies of the central line placement procedure, several observed limitations of the application had been observed and summarized as below that are worth improving.

1. The issue had been raised during the early phase pilot study that the virtual patient's upper body should be placed in a position where the head is turned to one side to guarantee the maximal exposure of IJV access from one side of the neck, by making it more prominent to identify the landmark of sternocleidomastoid. For the current implementation of the application, the CT dataset was scanned while the patient subject is standing straight up with the head facing forward without any tilting movement. One the one hand, the volume rendering is strictly carried out based on the input slice deck of the CT dataset, while depending on different anatomical structures, the neck does not have to be turned for the internal jugular vein to be maximally exposed. Additional model with the head turning to one side is recommended to add using the strict pipeline within the scope of this thesis.
2. Pulsation of the veins and arteries: As the generated 3-D volume is in the form of rigid body, it lacks the movement of the patient and internal tissue structures. In particular, for the CVC procedure simulation, the pulsation of the tissue needs to be further studied to

help identify the targeted region, also simulate the realistic physiological functionalities of the patients.

3. Needle tip interaction with the tissues in the ultrasound imagery: The novices who take on the initial training will find it difficult to properly place the inserted needle and visualize it in the ultrasound image. Indeed the overall trajectory of the advancing needle needs to be tracked to identify the precise location of the needle tip to determine whether the puncture has been established. Even though with the artificial indicator on the needle, there will be prompt feedback to indicate when the needle tip is in place, an additional "tenting" effect might be intuitive to the trainee, as the needle tip will cause a slight deformation of the surrounding tissues as it passes through the internal structures. This can be further studied and added into the composite ultrasound image while the interaction between the needle position with respect to the 3D volume, and the neighborhood area in two dimensional are both to be considered.
4. The haptic devices in the workspace will collide against each other during the simulation, as in the CVC procedure. The transducer needs to be placed closely to the insertion site of the needle in order to get a reachable perspective of the needle display, while collocation of the haptic proxy and the cursor in the scene are predefined. The stylus of the haptic interface should be properly redefined to avoid the mechanical collisions that will hinder the deeper needle penetration.
5. A patient library is needed for curriculum design: Currently only one patient's case is formulated for the surgical training for the IJV and subclavian approaches respectively. A complete and comprehensive curriculum should be created considering the difficulty of

vascular access because of the different pathological or anatomical structures of different patient. Hence, an effective assessment of skill transferability can be evaluated for the broad impact of the clinical demonstration.

CITED LITERATURE

[1] E. Wood and A. L. Loomis, "XXXVIII. The physical and biological effects of high-frequency sound-waves of great intensity," *The London, Edinburgh, and Dublin Philosophical Magazine and Journal of Science,* vol. 4, pp. 417-436, 1927.

[2] C. M. Tempany, N. J. McDannold, K. Hynynen, and F. A. Jolesz, "Focused ultrasound surgery in oncology: overview and principles," *Radiology,* vol. 259, pp. 39-56, 2011.

[3] D. H. Sheafor, E. K. Paulson, C. M. Simmons, D. M. DeLong, and R. C. Nelson, "Abdominal percutaneous interventional procedures: comparison of CT and US guidance," *Radiology,* vol. 207, pp. 705-710, 1998.

[4] R. M. Comeau, A. F. Sadikot, A. Fenster, and T. M. Peters, "Intraoperative ultrasound for guidance and tissue shift correction in image-guided neurosurgery," *Medical Physics,* vol. 27, p. 787, 2000.

[5] G. P. Penney, J. M. Blackall, D. Hayashi, T. Sabharwal, A. Adam, and D. J. Hawkes, "Overview of an ultrasound to CT or MR registration system for use in thermal ablation of liver metastases," in *Proc. Medical Image Understanding and Analysis*, 2001, p. 6568.

[6] T. Matalon and B. Silver, "US guidance of interventional procedures," *Radiology,* vol. 174, pp. 43-47, 1990.

[7] B. R. Douglas, J. W. Charboneau, and C. C. Reading, "Ultrasound-guided intervention: expanding horizons," *Radiologic Clinics of North America,* vol. 39, pp. 415-428, 2001.

[8] G. D. Dodd, C. C. Esola, D. S. Memel, A. A. Ghiatas, K. N. Chintapalli, E. K. Paulson, R. C. Nelson, J. V. Ferris, and R. L. Baron, "Sonography: the undiscovered jewel of interventional radiology," *Radiographics,* vol. 16, pp. 1271-1288, 1996.

[9] J. Del Cura, R. Zabala, and I. Corta, "US-guided interventional procedures: what a radiologist needs to know," *Radiología (English Edition),* vol. 52, pp. 198-207, 2010.

[10] É. Cardinal, R. K. Chhem, and C. G. Beauregard, "Ultrasound-guided interventional procedures in the musculoskeletal system," *Radiologic Clinics of North America,* vol. 36, pp. 597-604, 1998.

[11] D. W. Allen, P. S. Brady, and T. A. Matalon, "Ultrasound Guidance in Interventional Radiology," *Contemporary Diagnostic Radiology,* vol. 29, pp. 1-5, 2006.

[12] D. Aiger and D. Cohen-Or, "Real-time ultrasound imaging simulation," *Real-Time Imaging,* vol. 4, pp. 263-274, 1998.

[13] C. Terkamp, G. Kirchner, J. Wedemeyer, A. Dettmer, J. Kielstein, H. Reindell, J. Bleck, M. Manns, and M. Gebel, "Simulation of abdomen sonography. Evaluation of a new ultrasound simulator," *Ultraschall in der Medizin*, vol. 24, pp. 239-244, 2003.

[14] D. Henry, J. Troccaz, J.-L. Bosson, and O. Pichot, "Ultrasound imaging simulation: Application to the diagnosis of deep venous thromboses of lower limbs," in *Medical Image Computing and Computer-Assisted Interventation—MICCAI'98*, ed: Springer, 1998, pp. 1032-1040.

[15] J. A. Jensen, "Field: A program for simulating ultrasound systems," in *10TH NORDICBALTIC CONFERENCE ON BIOMEDICAL IMAGING, VOL. 4, SUPPLEMENT 1, PART 1: 351--353*, 1996.

[16] J. A. Jensen and N. B. Svendsen, "Calculation of pressure fields from arbitrarily shaped, apodized, and excited ultrasound transducers," *Ultrasonics, Ferroelectrics and Frequency Control, IEEE Transactions on*, vol. 39, pp. 262-267, 1992.

[17] L. MedSim Advanced Medical Simulations. (2008). *Ultrasim: Ultrasound training simulator*. Available: http://www.medsim.com/

[18] H.-H. Ehricke, "SONOSim3D: a multimedia system for sonography simulation and education with an extensible case database," *European journal of ultrasound*, vol. 7, pp. 225-230, 1998.

[19] H. Hoffman, D. Stredney, and S. Weghorst, "UltraTrainer-a training system for medical ultrasound examination," *Medicine Meets Virtual Reality: Art, Science, Technology: Healthcare (R) Evolution*, vol. 50, p. 298, 1998.

[20] M. Weidenbach, C. Wick, S. Pieper, K.-J. Quast, T. Fox, G. Grunst, and D. Redel, "Augmented reality simulator for training in two-dimensional echocardiography," *Computers and biomedical research*, vol. 33, pp. 11-22, 2000.

[21] I. Heer, K. Middendorf, S. Müller - Egloff, M. Dugas, and A. Strauss, "Ultrasound training: the virtual patient," *Ultrasound in obstetrics & gynecology*, vol. 24, pp. 440-444, 2004.

[22] A. M. Tahmasebi, K. Hashtrudi-Zaad, D. Thompson, and P. Abolmaesumi, "A framework for the design of a novel haptic-based medical training simulator," *Information Technology in Biomedicine, IEEE Transactions on*, vol. 12, pp. 658-666, 2008.

[23] R. Shams, R. Hartley, and N. Navab, "Real-time simulation of medical ultrasound from CT images," in *Medical Image Computing and Computer-Assisted Intervention–MICCAI 2008*, ed: Springer, 2008, pp. 734-741.

[24] O. Kutter, R. Shams, and N. Navab, "Visualization and GPU-accelerated simulation of medical ultrasound from CT images," *Computer methods and programs in biomedicine*, vol. 94, pp. 250-266, 2009.

[25] A. Hostettler, C. Forest, A. Forgione, L. Soler, and J. Marescaux, "Real-time ultrasonography simulator based on 3D CT-scan images," *Studies in Health Technology and Informatics*, vol. 111, pp. 191-193, 2005.

[26] F. P. Vidal, N. W. John, A. Healey, and D. A. Gould, "Simulation of ultrasound guided needle puncture using patient specific data with 3D textures and volume haptics," *Computer Animation and Virtual Worlds*, vol. 19, pp. 111-127, 2008.

[27] W. Wein, A. Khamene, D.-A. Clevert, O. Kutter, and N. Navab, "Simulation and fully automatic multimodal registration of medical ultrasound," in *Medical Image Computing and Computer-Assisted Intervention–MICCAI 2007*, ed: Springer, 2007, pp. 136-143.

[28] D. Magee, Y. Zhu, R. Ratnalingam, P. Gardner, and D. Kessel, "An augmented reality simulator for ultrasound guided needle placement training," *Medical & Biological Engineering & Computing*, vol. 45, pp. 957-967, 2007/10/01 2007.

[29] L. Yi-Je, J. Hu, C. Chu-Yin, and N. Tardella, "Soft Tissue Deformation and Cutting Simulation for the Multimodal Surgery Training," in *Computer-Based Medical Systems, 2006. CBMS 2006. 19th IEEE International Symposium on*, 2006, pp. 635-640.

[30] C. Forest, O. Comas, C. Vaysière, L. Soler, and J. Marescaux, "Ultrasound and needle insertion simulators built on real patient-based data," *Studies in Health Technology and Informatics*, vol. 125, p. 136, 2006.

[31] W. Wein, S. Brunke, A. Khamene, M. R. Callstrom, and N. Navab, "Automatic CT-ultrasound registration for diagnostic imaging and image-guided intervention," *Medical image analysis*, vol. 12, pp. 577-585, 2008.

[32] J. A. Jensen and I. Nikolov, "Fast simulation of ultrasound images," in *Ultrasonics Symposium, 2000 IEEE*, 2000, pp. 1721-1724.

[33] T. Reichl, J. Passenger, O. Acosta, and O. Salvado, "Ultrasound goes GPU: real-time simulation using CUDA," in *SPIE Medical Imaging*, 2009, pp. 726116-726116-10.

[34] S. I. Seldinger, "Catheter replacement of the needle in percutaneous arteriography; a new technique," *Acta radiol*, vol. 39, pp. 368-76, May 1953.

[35] Z. C. Higgs, D. A. Macafee, B. D. Braithwaite, and C. A. Maxwell-Armstrong, "The Seldinger technique: 50 years on," *Lancet*, vol. 366, pp. 1407-9, Oct 15-21 2005.

[36] K. K. Govindarajan, P. N. Bromley, and P. N. Bromley. (2014, Central Venous Access via Tunneled Anterior Approach to Internal Jugular Vein. *Medscape*. Available: http://emedicine.medscape.com/article/80298-overview#showall

[37] M. Slama, A. Novara, A. Safavian, M. Ossart, M. Safar, and J. Y. Fagon, "Improvement of internal jugular vein cannulation using an ultrasound-guided technique," *Intensive Care Med*, vol. 23, pp. 916-9, Aug 1997.

[38] B. G. Denys, B. F. Uretsky, and P. S. Reddy, "Ultrasound-assisted cannulation of the internal jugular vein. A prospective comparison to the external landmark-guided technique," *Circulation*, vol. 87, pp. 1557-62, May 1993.

[39] E. J. Yang, H. S. Ha, Y. H. Kong, and S. J. Kim, "Ultrasound-guided internal jugular vein catheterization in critically ill pediatric patients," *Korean J Pediatr*, vol. 58, pp. 136-41, Apr 2015.

[40] H. Dolu, S. Goksu, L. Sahin, O. Ozen, and L. Eken, "Comparison of an ultrasound-guided technique versus a landmark-guided technique for internal jugular vein cannulation," *J Clin Monit Comput*, vol. 29, pp. 177-82, Feb 2015.

[41] P. S. Calhoun, B. S. Kuszyk, D. G. Heath, J. C. Carley, and E. K. Fishman, "Three-dimensional Volume Rendering of Spiral CT Data: Theory and Method," *RadioGraphics*, vol. 19, pp. 745-764, 1999.

[42] A. Kaufman, D. Cohen, and R. Yagel, "Volume Graphics," *Computer*, vol. 26, pp. 51-64, 1993.

[43] M. Hadwiger, J. M. Kniss, C. Rezk-salama, D. Weiskopf, and K. Engel, *Real-time Volume Graphics*: A. K. Peters, Ltd., 2006.

[44] Kitware. (2015). *Volview Toolkit*. Available: http://www.kitware.com/opensource/volview.html

[45] F. P. Vidal, F. Bello, K. W. Brodlie, N. W. John, D. Gould, R. Phillips, and N. J. Avis, "Principles and Applications of Computer Graphics in Medicine," *Computer Graphics Forum*, vol. 25, pp. 113-137, 2006.

[46] W. E. Lorensen and H. E. Cline, "Marching cubes: A high resolution 3D surface construction algorithm," *SIGGRAPH Comput. Graph.*, vol. 21, pp. 163-169, 1987.

[47] W. E. Lorensen and H. E. Cline, "Marching cubes: A high resolution 3D surface construction algorithm," presented at the Proceedings of the 14th annual conference on Computer graphics and interactive techniques, 1987.

[48] T. S. Newman and H. Yi, "A survey of the marching cubes algorithm," *Computers & Graphics*, vol. 30, pp. 854-879, 2006.

[49] M. G. Silk, *Ultrasonic transducers for nondestructive testing*, 1984.

[50] T. Gulrez, A. Tognetti, and D. De Rossi, "Sensorized Garment Augmented 3D Pervasive Virtual Reality System," in *Pervasive Computing*, A.-E. Hassanien, J. H. Abawajy, A. Abraham, and H. Hagras, Eds., ed: Springer London, 2010, pp. 97-115.

[51] OSG Community. (2006, May 26). *OpenSceneGraph*. Available: http://www.openscenegraph.org

[52] OpenSG Forum. (May 26th). *OpenSG*. Available: http://sourceforge.net/projects/opensg/

[53] A. L. Ames, D. R. Nadeau, and J. L. Moreland, *VRML 2.0 sourcebook*. New York, N.Y. [etc.]: Wiley, 1997.

[54] W. D. Consortium. (1999, May 26th). *Open Standards for Real-Time 3D Communication*. Available: http://www.web3d.org/

[55] SGI. (May 24th). *Open Inventor*. Available: oss.sgi.com/projects/inventor/

[56] P. N. T. Wells and H.-D. Liang, "Medical ultrasound: imaging of soft tissue strain and elasticity," *Journal of The Royal Society Interface*, vol. 8, pp. 1521-1549, 2011.

[57] K. Thangavel, R. Manavalan, and I. L. Aroquiaraj, "Removal of speckle noise from ultrasound medical image based on special filters: comparative study," *ICGST-GVIP Journal*, vol. 9, pp. 25-32, 2009.

[58] K. K. Shung and G. A. Thieme, *Ultrasonic Scattering in Biological Tissues*: CRC Press, 1992.

[59] M. E. Lyons, R. C. Chivers, and K. J. Parker, "Absorption Dominates Attenuation in Soft Tissues," in *IEEE 1986 Ultrasonics Symposium*, 1986, pp. 871-874.

[60] B. Oosterveld, J. Thijssen, P. Hartman, R. Romijn, and G. Rosenbusch, "Ultrasound attenuation and texture analysis of diffuse liver disease: methods and preliminary results," *Physics in medicine and biology*, vol. 36, p. 1039, 1991.

[61] L. Wilson, D. Robinson, and B. Doust, "Frequency domain processing for ultrasonic attenuation measurement in liver," *Ultrasonic imaging*, vol. 6, pp. 278-292, 1984.

[62] R. Kuc, "Clinical Application of an Ultrasound Attenuation Coefficient Estimation Technique for Liver Pathology Characterization," *Biomedical Engineering, IEEE Transactions on*, vol. BME-27, pp. 312-319, 1980.

[63] D. J. Dowsett, P. Kenny, and R. E. Johnston, *The Physics of Diagnostic Imaging*: Chapman & Hall Medical, 1988.

[64] Y. Zhu, D. R. Magee, D. Kessel, and R. Ratnalingam, "A Virtual Ultrasound Imaging System for the Simulation of Ultrasound-Guided Needle Insertion Procedures," in *Proc. Medical Image Understanding and Analysis*, 2006, pp. 61-65.

[65] K. Perlin, "Improving noise," *ACM Trans. Graph.*, vol. 21, pp. 681-682, 2002.

[66] K. Perlin, "An image synthesizer," *SIGGRAPH Comput. Graph.*, vol. 19, pp. 287-296, 1985.

[67] K. Perlin and E. M. Hoffert, "Hypertexture," *SIGGRAPH Comput. Graph.*, vol. 23, pp. 253-262, 1989.

[68] M. Zucker. (2001, May 24). *The Perlin Noise Math FAQ*.

[69] K. A. Carmody, C. L. Moore, and D. Feller-Kopman, *Handbook of Critical Care and Emergency Ultrasound*: McGraw-Hill Education, LLC, 2011.

[70] D. W. Allen, P. S. Brady, and T. A. S. Matalon, "Ultrasound Guidance in Interventional Radiology," *Contemporary Diagnostic Radiology*, vol. 29, pp. 1-5, 2006.

[71] D. Katz and L. E. Krueger, *The World of Touch*. Hillsdale, NJ: Lawrence Erlbaum Associates, 1989.

[72] E. P. Scilingo, M. Bianchi, G. Grioli, and A. Bicchi, "Rendering Softness: Integration of Kinesthetic and Cutaneous Information in a Haptic Device," *Haptics, IEEE Transactions on*, vol. 3, pp. 109-118, 2010.

[73] A. Kheddar, A. Drif, J. Citérin, and B. L. Mercier, "A multi-level haptic rendering concept," in *Proceedings of EuroHaptics 2004*, Munich, Germany, 2004.

[74] Y.-U. Song and J.-H. Ryu, "A Study on Unconstrained Tactile-Kinesthetic Feedback," in *2012 9th International Conference on Ubiquitous Robots and Ambient Intelligence (URAI)*, Daejeon, Korea, 2012.

[75] A. Khatchatourov, J. Castet, J.-L. Florens, A. Luciani, and C. Lenay, "Integrating tactile and force feedback for highly dynamic tasks: Technological, experimental and epistemological aspects," *Interacting with Computers*, vol. 21, pp. 26-37, 2009.

[76] H. Farley, Steel, C.H., "A quest for the holy grail: Tactile percision, natural movement and haptic feedback in 3D virtual spaces," in *Same places, different spaces*, Auckland, New Zealand, 2009, pp. 285-295.

[77] F. G. Hamza-Lup, C. M. Bogdan, D. M. Popovici, and O. D. Costea, "A Survey of Visuo-Haptic Simulation in Surgical Training," Gosier, Guadeloupe, France, 2011, pp. 57-62.

[78] D. Chen. (2008, Haptics for Touch-Enabled Simulation and Training. *Patient Safety & Quality Health Care*.

[79] S. Wall, "An Investigation of Temporal and Spatial Limitations of Haptic Interfaces," PhD thesis, Department of Cybernetics, University of Reading.

[80] Sensable Technologies. (Since 1993). Available: www.Sensable.com and www.Sensabledental.com

[81] Geomagic. (2015). Available: http://www.geomagic.com/en/

[82] Mimic Technologies. (Since 2001). Available: http://www.mimicsimulation.com/

[83] Force Dimension. (Since 2001). Available: http://www.forcedimension.com/

[84] Novint. (2012). Available: http://www.novint.com/

[85] P. Kadleček. and P. Kmoch., "Overview of current developments in haptic APIs," in *Proceedings of CESCG 2011: The 15th Central European Seminar on Computer Graphics*, 2011.

[86] F. B. Francois Conti, Dan Morris, and Christopher Sewell, "CHAI 3D: An Open-Source Library for the Rapid Development of Haptic Scenes," presented at the IEEE World Haptics, Pisa, Italy, 2005.

[87] Stanford Artificial Intelligence Lab (SAIL). (Since 1962). Available: http://ai.stanford.edu/

[88] SenseGraphics AB. *H3D*. Available: http://www.h3dapi.org/

[89] SenseGraphics AB. (2015). Available: http://www.sensegraphics.com/

[90] VRlab Umeå University. (since 2003). *OpenSceneGrapgh Haptic Library*. Available: http://sourceforge.net/projects/osghaptics/

[91] ReachIn Technologies AB. *Reachin API*. Available: http://www.reachin.se/products/ReachinAPI

[92] ReachIn Technologies AB. (2015). Available: http://www.reachin.se/

[93] R. J. Rost, *OpenGL Shading Language, Second Edition*: Addison Wesley Professional, 2006.

[94] 3Dconnexion. Available: http://www.3dconnexion.com/

[95] SensAble. (2015). *OpenHaptics software development toolkit*. Available: http://www.geomagic.com/en/products/open-haptics/overview/

[96] SensAble. (2015). *Academic Edition of OpenHaptics v3.0 with QuickHaptics*. Available: http://www.dentsable.com/products-openhaptics-toolkit.htm

[97] M. N. Gallagher AG1, McGuigan J, Ritchie K, Sheehy NP., "An Ergonomic Analysis of the Fulcrum Effect in the Acquisition of Endoscopic Skills," *Endoscopy*, vol. 30, pp. 617-620, 1998.

[98] G. A. Crothers IR, McClure N, James DT, McGuigan J., "Experienced Laparoscopic Surgeons are Automated to the "Fulcrum Effect": An Ergonomic Demonstration," *Endoscopy,* vol. 31, pp. 365-369, 1999.

[99] F. T. Smith CD, McNatt SS, Metreveli RE., "Assessing laparoscopic manipulative skills," *The American Journal of Surgery*, vol. 181, pp. 547-550, 2001.

[100] E. P. W. v. d. Putten, R. H. M. Goossens, J. J. Jakimowicz, and J. Dankelman, "Haptics in minimally invasive surgery – a review," *Minimally Invasive Therapy & Allied Technologies.*, vol. 17, pp. 3-16, 2008.

[101] C. Luciano, P. Banerjee, and T. DeFanti, "Haptics-based virtual reality periodontal training simulator," *Virtual Reality*, vol. 13, pp. 69-85, 2009.

[102] A. L. Hewlett and M. E. Rupp, "New Developments in the Prevention of Intravascular Catheter Associated Infections," *Infectious Disease Clinics of North America*, vol. 26, pp. 1-11, 2012.

[103] T. J. Hoff and C. Soerensen, "No Payment for Preventable Complications: Reviewing the Early Literature for Content, Guidance, and Impressions," *Quality Management in Healthcare*, vol. 20, pp. 62-75, 2011.

[104] A. Zaghal, M. Khalife, D. Mukherji, N. El Majzoub, A. Shamseddine, J. Hoballah, G. Marangoni, and W. Faraj, "Update on totally implantable venous access devices," *Surgical Oncology*, vol. 21, pp. 207-215, 2012.

[105] D. C. McGee and M. K. Gould, "Preventing Complications of Central Venous Catheterization," *New England Journal of Medicine*, vol. 348, pp. 1123-1133, 2003.

[106] I. Raad, D. C. Hohn, B. J. Gilbreath, N. Suleiman, L. A. Hill, P. A. Bruso, K. Marts, P. F. Mansfield, and G. P. Bodey, "Prevention of central venous catheter-related infections by using maximal sterile barrier precautions during insertion," *Infect Control Hosp Epidemiol*, vol. 15, pp. 231-8, 1994.

[107] J. F. Timsit, J. C. Farkas, J. M. Boyer, J. B. Martin, B. Misset, B. Renaud, and J. Carlet, "Central vein catheter-related thrombosis in intensive care patients: incidence, risks factors, and relationship with catheter-related sepsis," *Chest*, vol. 114, pp. 207-13, Jul 1998.

[108] K. B. Domino, T. A. Bowdle, K. L. Posner, P. H. Spitellie, L. A. Lee, and F. W. Cheney, "Injuries and liability related to central vascular catheters: a closed claims analysis," *Anesthesiology*, vol. 100, pp. 1411-8, Jun 2004.

[109] C. S. Ezaru, M. P. Mangione, T. M. Oravitz, J. W. Ibinson, and R. J. Bjerke, "Eliminating arterial injury during central venous catheterization using manometry," *Anesth Analg*, vol. 109, pp. 130-4, Jul 2009.

[110] D. R. Jobes, A. J. Schwartz, D. E. Greenhow, L. W. Stephenson, and N. Ellison, "Safer jugular vein cannulation: recognition of arterial puncture and preferential use of the external jugular route," *Anesthesiology*, vol. 59, pp. 353-5, Oct 1983.

[111] W. C. Oliver, Jr., G. A. Nuttall, F. M. Beynen, H. S. Raimundo, J. P. Abenstein, and J. J. Arnold, "The incidence of artery puncture with central venous cannulation using a modified technique for detection and prevention of arterial cannulation," *J Cardiothorac Vasc Anesth*, vol. 11, pp. 851-5, Dec 1997.

[112] C. A. Troianos, D. R. Jobes, and N. Ellison, "Ultrasound-guided cannulation of the internal jugular vein. A prospective, randomized study," *Anesth Analg*, vol. 72, pp. 823-6, Jun 1991.

[113] M. Blaivas and S. Adhikari, "An unseen danger: frequency of posterior vessel wall penetration by needles during attempts to place internal jugular vein central catheters using ultrasound guidance," *Crit Care Med*, vol. 37, pp. 2345-9; quiz 2359, Aug 2009.

[114] S. Tsuda, D. Scott, J. Doyle, and D. B. Jones, "Surgical skills training and simulation," *Curr Probl Surg*, vol. 46, pp. 271-370, Apr 2009.

APPENDIX

VIRTUAL CENTRAL VENOUS CATHETER FEEDBACK QUESTIONNAIRE

Date:_____

Please help us improve this simulator by sharing your feedback.

1. What is your specialty?

Internal Med Emergency Med Radiology Anesthesia Surgery Other: _____

2. Year of training:

☐ PGY1 ☐PGY2 ☐ PGY3 ☐ PGY4 ☐ PGY5 ☐ PGY6

OR ___ Years since completed residency

3. How many total central venous catheter placements have you performed…

a. In the <u>last 12 months</u>?

$_0$☐0 $_1$☐1-5 $_2$☐6-10 $_3$☐11-15 $_4$☐16-20 $_5$☐21-30 $_6$☐31-40 $_7$☐41-50 $_8$☐>50

b. <u>Ever</u>?

$_0$☐0 $_1$☐1-5 $_2$☐6-10 $_3$☐11-15 $_4$☐16-20 $_5$☐21-30 $_6$☐31-40 $_7$☐41-50 $_8$☐>50

1. How **realistic** was the image of the virtual patient's head and neck?

1	2	3	4	5
Not at all realistic	Somewhat realistic	Realistic	Very realistic	Extremely realistic

Comments:

2. How **accurate** was the internal anatomy?

1	2	3	4	5
Not at all realistic	Somewhat realistic	Realistic	Very realistic	Extremely realistic

Comments:

3. How **realistic** was the stylus as a simulation of a central venous catheter needle (e.g., hand position while holding, weight in hand, freedom of motion)?

1	2	3	4	5
Not at all realistic	Somewhat realistic	Realistic	Very realistic	Extremely realistic

Comments:

4. How **realistic** was the stylus as a simulation of an ultrasound transducer (e.g., hand position while holding, weight in hand, freedom of motion)?

1	2	3	4	5
Not at all realistic	Somewhat realistic	Realistic	Very realistic	Extremely realistic

Comments:

1. How **realistic** was the haptic sensation when puncturing the skin?

1	2	3	4	5
Not at all realistic	Somewhat realistic	Realistic	Very realistic	Extremely realistic

Comments:

2. How **difficult** was it to use both styli together?

1	2	3	4	5
Not at all difficult	Somewhat difficult	Moderately difficult	Very difficult	Extremely difficult

Comments:

1. How important are each of the following simulator attributes for effective simulation-based training of central venous catheter placement?

	Unimportant		Moderately important		Extremely important
Realism of the virtual image	1	2	3	4	5
Accuracy of internal anatomy	1	2	3	4	5
Realism of the stylus as a simulator of a needle	1	2	3	4	5
Realism of the stylus as a stimulator of an ultrasound transducer	1	2	3	4	5
Realistic haptic sensation when puncturing the skin	1	2	3	4	5

2. How **helpful** would it be for students and residents to practice central venous catheter placement on this simulator?

1	2	3	4	5
Not at all helpful	Somewhat helpful	Helpful	Very helpful	Extremely helpful

Comments:

What changes or features would make this model more useful for learning to perform central venous catheter placement?